



LAWRENCE
LIVERMORE
NATIONAL
LABORATORY

LLNL-JRNL-523436

Cryogenic thermonuclear fuel implosions on the National Ignition Facility

S. H. Glenzer, D. Callahan, A. J. Mackinnon, J. L. Kline, G. Grim, E. T. Alger, L. Bernstein, R. Betti, D. L. Bleuel, T. R. Boehly, D. K. Bradley, S. C. Burkhart, R. Burr, J. Caggiano, C. Castro, D. T. Casey, C. Choate, D. S. Clark, P. Cellierss, C. Cerjan, G. W. Collins, E. L. Dewald, P. DiNicola, M. M. DiNicola, L. Divol, S. Dixit, T. Doeppner, R. Dylla-Spears, E. Dzenitis, M. Eckart, G. Erbert, D. Farley, J. Fair, D. Fittingjoff, L. J. Frenje, S. Friedrich, M. Gatu Johnson, C. Gibson, E. Giraldez, V. Glebov, S. Glenn, S. W. Haan, B. J. Haid, B. A. Hammel, A. V. Hamza, C. A. Haynam, G. M. Heestand, M. Hermann, H. Hermann, D. G. Hicks, D. E. Hinkel, J. P. Holder, D. M. Holunda, J. B. Horner, W. Hsing, H. Huang, N. Izumi, M. Jackson, O. S. Jones, et al.

January 19, 2012

Physics of Plasma

Disclaimer

This document was prepared as an account of work sponsored by an agency of the United States government. Neither the United States government nor Lawrence Livermore National Security, LLC, nor any of their employees makes any warranty, expressed or implied, or assumes any legal liability or responsibility for the accuracy, completeness, or usefulness of any information, apparatus, product, or process disclosed, or represents that its use would not infringe privately owned rights. Reference herein to any specific commercial product, process, or service by trade name, trademark, manufacturer, or otherwise does not necessarily constitute or imply its endorsement, recommendation, or favoring by the United States government or Lawrence Livermore National Security, LLC. The views and opinions of authors expressed herein do not necessarily state or reflect those of the United States government or Lawrence Livermore National Security, LLC, and shall not be used for advertising or product endorsement purposes.

Cryogenic thermonuclear fuel implosions on the National Ignition Facility

S. H. Glenzer¹, D. A. Callahan¹, A. J. MacKinnon¹, J. L. Kline², G. Grim², E. T. Alger¹, R. Betti³, D. L. Bleuel¹, T. R. Boehly³, D. K. Bradley¹, S. C. Burkhardt¹, R. Burr¹, J. A. Caggiano¹, C. Castro¹, D. T. Casey⁴, C. Choate¹, D. S. Clark¹, P. Celliers¹, C. J. Cerjan¹, G. W. Collins¹, E. L. Dewald¹, P. DiNicola¹, J. M. DiNicola¹, L. Divol¹, S. Dixit¹, T. Döppner¹, R. Dylla-Spears¹, E. Dzenitis¹, M. Eckart¹, G. Erbert¹, D. Farley¹, J. Fair¹, D. Fittinghoff², L. J. A. Frenje⁴, S. Friedrich¹, D.T Casey⁴, M. Gatu Johnson⁴, C. Gibson¹, E. Giraldez¹, V. Glebov³, S. Glenn¹, S. W. Haan¹, B. J. Haid¹, B. A. Hammel¹, A. V. Hamza¹, C. A. Haynam¹, G. M. Heestand¹, M. Hermann¹, H. W. Hermann¹, D. G. Hicks¹, D. E. Hinkel¹, J. P. Holder¹, D. M. Holunda¹, J. B. Horner¹, W. W. Hsing¹, H. Huang¹, N. Izumi¹, M. Jackson¹, O. S. Jones¹, D. H. Kalantar¹, R. Kauffman¹, J. D. Kilkenny⁵, R. K. Kirkwood¹, J. Klingmann¹, T. Kohut¹, J. P. Knauer³, J. A. Koch¹, B. Kozioziemki¹, G. A. Kyrala², J. Kroll¹, K. La Fortune¹, L. Lagin¹, O. L. Landen¹, D. W. Larson¹, D. LaTray¹, R. J. Leeper⁶, S. Le Pape¹, J. D. Lindl¹, R. Lowe-Webb¹, T. Ma¹, J. McNaney¹, A. G. MacPhee¹, T. N. Malsbury¹, E. Mapoles¹, C. D. Marshall¹, N. B. Meezan¹, F. Merrill², P. Michel¹, J. D. Moody¹, A. S. Moore⁷, M. Moran¹, K. A. Moreno¹, D. H. Munro¹, B. R. Nathan¹, A. Nikroo⁵, R. E. Olson⁶, C. D. Orth¹, A. E. Pak¹, P. K. Patel¹, T. Parham¹, R. Petrasso³, J. E. Ralph¹, H. Rinderknecht⁴, S. P. Regan³, H. F. Robey¹, J. S. Ross¹, M. D. Rosen¹, R. Sacks¹, J. D. Salmonson¹, R. Saunders¹, J. Sater¹, C. Sangster³, M. B. Schneider¹, F. H. Séguin⁴, M. J. Shaw¹, B. K. Spears¹, P. T. Springer¹, W. Stoeffl¹, L. J. Suter¹, C. A. Thomas¹, R. Tommasini¹, R. P. J. Town¹, C. Walters¹, S. Weaver¹, S. V. Weber¹, P. J. Wegner¹, P. K. Whitman¹, K. Widmann¹, C. C. Widmayer¹, D. C. Wilson², B. Van Wonterghem¹, B. J. MacGowan¹, L. J. Atherton¹, M. J. Edwards¹, and E. I. Moses¹

¹Lawrence Livermore National Laboratory, Livermore, CA 94550, USA

²Los Alamos National Laboratory, Los Alamos, NM 87545, USA

³Laboratory for Laser Energetics, University of Rochester, Rochester, NY 14623, USA

⁴Plasma Fusion Science Center, Massachusetts, Institute of Science and Technologie, Cambridge, MA 02139, USA

⁵General Atomics, San Diego, CA , USA

⁶Sandia National Laboratory, Sandia, NM 87185, USA and

⁷Atomic Weapons Establishment, Aldermaston, RG7, UK

The first inertial confinement fusion implosion experiments with equimolar deuterium-tritium thermonuclear fuel have been performed on the National Ignition Facility. These experiments use 0.17 mg of fuel with the potential for ignition and significant fusion yield conditions. The thermonuclear fuel has been fielded as a cryogenic layer on the inside of a spherical plastic capsule that is mounted in the center of a cylindrical gold hohlraum. Heating the hohlraum with 192 laser beams for a total laser energy of 1.6 mega joules produces a soft x-ray field with 300 eV temperature. The ablation pressure produced by the radiation field compresses the initially 2.2-mm diameter capsule by a factor of 30 to a spherical dense fuel shell that surrounds a central hot-spot plasma of 50 μm diameter. While an extensive set of x-ray and neutron diagnostics has been applied to characterize hot spot formation from the x-ray emission and 14.1 MeV deuterium-tritium primary fusion neutrons, thermonuclear fuel assembly is studied by measuring the down-scattered neutrons with energies in the range of 10 to 12 MeV. X-ray and neutron imaging of the compressed core and fuel indicate a fuel thickness of $(14 \pm 3) \mu\text{m}$, which combined with magnetic recoil spectrometer measurements of the fuel areal density of $(1 \pm 0.09) \text{ g cm}^{-2}$ result in fuel densities approaching 600 g cm^{-3} . The fuel surrounds a hot-spot plasma with average ion temperatures of $(3.5 \pm 0.1) \text{ keV}$ that is measured with neutron time of flight spectra. Absolute neutron yields of $(7.5 \pm 0.1) \times 10^{14}$ have been recorded from the magnetic recoil spectrometer and nuclear activation diagnostics while gamma ray measurements provide the duration of nuclear activity of $(170 \pm 30) \text{ ps}$. These indirect-drive implosions result in the highest areal densities and neutron yields achieved on laser facilities to date. This achievement is the result of the first hohlraum and capsule tuning experiments where the stagnation pressures have been systematically increased by more than a factor of 10 by fielding low-entropy implosions through the control of radiation symmetry, small hot electron production, and proper shock timing. The stagnation pressure is above 100 Gbar resulting in high Lawson confinement parameters of $P\tau \simeq 10 \text{ atm s}$. Comparisons with radiation-hydrodynamic simulations indicate that the pressure is within a factor of three required for reaching ignition and high yield. This will be the focus of future higher-velocity implosions that will employ additional optimizations of hohlraum, capsule and laser pulse shape conditions.

I. INTRODUCTION

Inertial confinement fusion (ICF) experiments compress a shell capsule containing a deuterium-tritium ice

layer in a high-velocity, low-entropy implosion to form a central hot spot plasma that is surrounded by the

high-density nuclear fuel. When the hot spot reaches sufficiently high densities and temperatures from a combination of PdV work and alpha particle deposition, a nuclear burn wave is launched igniting the surrounding dense fuel, sustained by alpha deposition and electron conduction without an external energy source [1–4]. This threshold behavior for ignition and burn is predicted in simulations when reaching stagnation pressures above 300 Gbar.

Current indirectly driven fusion capsule implosions are performed on the National Ignition Facility to approach these conditions [5–8]. In these experiments, the thermonuclear fuel is initially prepared cryogenically into a solid ice layer of hydrogen isotopes on the inside of a low-Z (plastic) ablator and fielded in the center of a radiation cavity called hohlraum. The implosion is driven by a spherical soft x-radiation drive from a 300 eV hohlraum that is heated with up to 1.6 mega joules of laser energy at peak laser power of 430 TW. The radiation field generates ablation pressures in excess of 100 MBar resulting in a rocket-like acceleration of the shell compressing the capsule toward the center with the goal to produce a central hot spot plasma that is surrounded by dense thermonuclear fuel with densities of 1000 g/cm³.

Near peak compression when the imploding fuel has converted most of the kinetic energy to internal energy, temperatures of about 4 keV must be reached in the hot spot and the fuel must reach high areal densities of > 1 g cm⁻². In these conditions, α -heating is expected to launch a self propagating burn wave that will heat the plasma to temperature above 10 keV and overwhelm cooling by expansion and electron conduction. The loss and expansion rates are of order 100 ps and drive the time during which most of the burn must occur. For example, burning approximately 1/3 of the DT-fuel will result into 6.5×10^{18} fusion neutrons with a total neutron yield of 15 mega joules and a gain value approaching 10.

Several forms of a generalized Lawson criterion [9–12] have been developed to assess progress towards ignition. For ICF, hot spot formation and thermonuclear fuel assembly can be characterized by the neutron yield from primary deuterium-tritium reactions in the central hot plasma, $D + T = ^4\text{He}(3.5 \text{ MeV}) + n(14.1 \text{ MeV})$, and the ratio of down scattered to primary neutrons, $N(10 - 12 \text{ MeV})/N(13 - 15 \text{ MeV})$, quantifying neutrons that have lost energy by scattering processes in the dense fuel plasma that surrounds the central hot plasma. These measured quantities are combined into an experimental ignition threshold factor [13, 14] that shows a 50 % probability for ignition for non-burn values of the DT equivalent fusion yield of $Y_{DT} = 3.2 \times 10^{15}$ and a down scattered ratio of 7 %.

The first layered implosion experiments with thermonuclear fuel [15, 16] have followed commissioning of the National Ignition Facility (NIF) [17, 18] and the demonstration of hohlraum symmetry [19–21] with adequate soft x-ray drive [5, 22]. In addition, a suite of tuning experiments have been commissioned [6, 23–30]

to measure and control [31, 32] four key capsule performance parameters: drive symmetry during the foot and the peak of the laser pulse, shock timing, peak implosion velocity, and hydrodynamic mix. Layered implosions have since then been routinely fielded to measure performance and to indicate progress towards our goal to field a fusion experiment that uses equimolar Deuterium-Tritium (DT) fill and that has a high probability for achieving ignition and burn.

The layered implosion experiments use equimolar mixtures of DT or diluted fuel with Tritium, Hydrogen and Deuterium (THD) [8]. The fuel is layered in 2.26 mm-diameter CH capsules in a $(68 \pm 1) \mu\text{m}$ thick layer; currently, more than 40 % of the layered experiments have been performed with fuel ice layer characteristics that meet the specifications for ignition [33]. Fielding these layers with adequate laser power balance and laser pulse shaping [18] have resulted in near symmetric compression to a sphere with a central hot-spot diameter of 50 μm and a fuel shell of about 80 μm . These indirect-drive implosion demonstrate the highest neutron yields of $(7.5 \pm 0.1) \times 10^{14}$ and areal densities of $(1 \pm 0.09) \text{ g cm}^{-2}$ achieved to date in laser experiments.

The paper is organized as follows. Section 2 describes the hohlraum and capsule targets together with fuel layer capabilities on NIF. An example of a groove analysis for a cryogenic fuel layer used for shot selection is also provided. Section 3 describes the laser drive and soft x-ray production in the hohlraum that resulted in implosion velocities of 95 % of the ignition value. Section 4 presents the resulting capsule implosion symmetry and core shape that approximately meet ignition requirements. Improvements in areal density and entropy due to implementation of adequate shock timing are described in Sec. 5. These values are within 30 % of the ignition-required value. Section 6 describes nuclear performance data from cryogenic layered implosion experiments indicating accurate measurements of the experimental ignition threshold factor. This analysis shows that layered implosions approach the ignition regime after each successive tuning experiments. Section 7 provides estimates of the averaged stagnation pressure from hot spot formation and nuclear fuel assembly data. A generalized Lawson confinement parameter is utilized indicating that a factor of three increase in pressure is needed to reach the ignition regime. Section 8 presents the conclusions and an outlook to future experiments that outline future improvements with the goal to reach the ignition regime.

II. INERTIAL CONFINEMENT FUSION TARGETS

Figure 1 shows a schematic of the hohlraum, capsule, and nuclear fuel ice layer employed in these experiments. The thermonuclear fuel is prepared cryogenically in a layer inside a 2.26 mm diameter plastic capsule, which is doped with Si or Ge. The dopant absorbs high en-

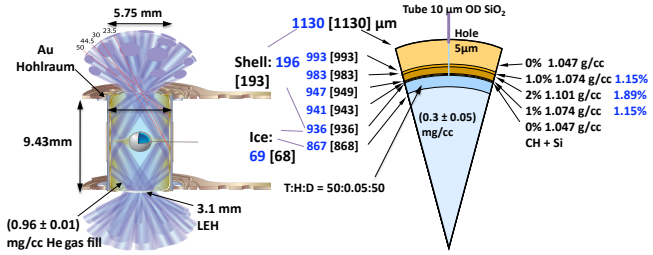


FIG. 1: (left) Schematic of an ignition scale hohlraum is shown along with (right) a fusion capsule that contains a $(68 \pm 1)\mu\text{m}$ -thick deuterium-tritium ice layer. The capsule consists of five plastic layers of various thickness, three of which are doped with nominal 1 %, 2 %, and 1 % Si per mass units. On the inside of the ablator, the ice layer contains most of the nuclear fuel. The numbers in black show the nominal dimensions and numbers in blue show actual as-fielded dimensions for the system shot N110914.

ergy x-rays from the laser-driven gold hohlraum and is used to tailor the density gradient at the ablator-ice interface. During the cryogenic layering process the target is fully enclosed by a shroud to protect it from chamber thermal radiation as well as from gaseous impurities that condense on cold surfaces. Additional protection from ice condensates during layering and during the final exposure to the target chamber atmosphere is further provided by the laser entrance hole (LEH) thermally isolated secondary windows [15, 23].

A smooth solid fuel layer is produced with the technique known as beta layering [34–36]. With frozen fuel in the fill tube and liquid at the bottom of the fusion capsule, a small drop of the capsule temperature by 45 mK provides a seed for growing the capsule ice layer with the correct orientation [33]. The seed is initially in an unstable fcc ice phase which converts to hcp crystals. Layering is started at a temperature of 100 mK below the triple point, for example $T_{\text{triple}} \simeq 19.6$ K for DT, and slowly cooled to about 400 mK below the triple point over a period of 14 to 18 hours during which the radioactive self heating from beta decay in the condensed fuel enables redistribution of the solid along the isotherms in the capsule.

The target is shot with a nominal temperature of $\Delta T = -1.5$ K or $\Delta T = -0.8$ K below the triple point. This temperature is reached a few seconds before the system shot by lowering the target temperature from the temperature at the end of the layering process over a period of a 30 second-long quench. The shroud opens close to the end of the quench and 8 seconds before the laser beams are fired; a small increase in temperature due to exposure to thermal radiation of about 400 mK is compensated for so that the final temperature is reached about 5 seconds before the shot.

At the cryogenic shot temperature, the scale-575 gold hohlraums are 9.43 mm long with a diameter of 5.75 mm and filled with helium gas at a pressure of 260 ± 2.5 torr

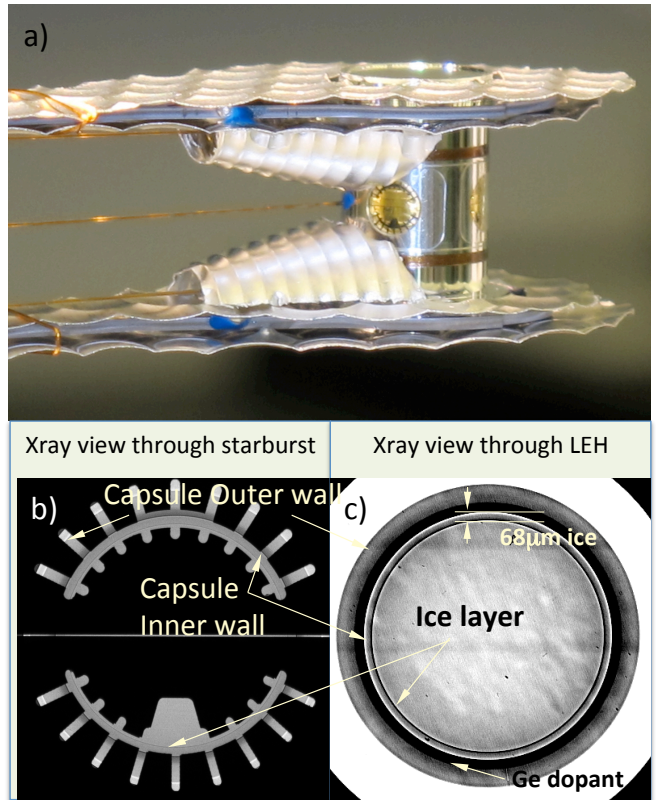


FIG. 2: (a) Picture of a cryogenic ignition target before it is fully enclosed by a shroud. On the side of the hohlraum, a cutout can be identified which is covered with a 10 nm thick Au coating and that allows characterization of the ice fuel layer during the layering process. X-ray radiographic images of the capsule and thermonuclear fuel layer seen (b) through the star burst and (c) through the laser entrance hole with phase contrast enhanced imaging.

resulting in densities of 0.96 mg cm^{-3} . Earlier hohlraum dimensions for Ge-doped capsule implosions were slightly different with a smaller diameter of 5.44 mm and length of 1.01 mm. In addition, hohlraums with two different Laser Entrance Hole (LEH) diameters of 3.1 mm and 3.375 mm have been fielded. These modification have been performed to study and improve implosion symmetry at high drive laser energy.

Figure 2 shows an ignition hohlraum target mounted on the cryogenic target positioner before being enclosed by a shroud. Also shown is the fuel distribution inside the capsule measured with 9 keV x-ray point projection radiography using a tungsten L-emission source. Characterization is routinely performed along 3 lines of sight with an axial view through the laser entrance holes and 2 orthogonal views, cf. Fig. 2(b). The latter are obtained in the equatorial plane through the starburst cut outs in the hohlraum cylinder walls that can be identified in Fig. 2(a). In addition, low magnification images are taken that provide an estimate of the total groove area by phase contrast enhanced imaging of groove defects [37]. This

powerful technique has been shown to detect small but deep grooves in the part of the layer that is not diagnosed with images at standard magnification, see comparison between Fig. 2 (b) and (c).

For the DT layer shown in Fig. 2(c) only a small groove can be identified with a length of $86.0\mu\text{m}$, width of $15.0\mu\text{m}$, depth of $2.4\mu\text{m}$. Estimates of the total effect of grooves on hot spot non uniformities takes into account the sum over all defects of area A and length L , $K = \sqrt{\frac{1}{V_{\text{fuel}}} \sum_{j=1}^n A_j^2 L_j}$, where we require $A \leq 250\mu\text{m}^2$ to avoid a groove from breaking through the layer during the implosion. This analysis indicates that the layer is of ignition quality with a total groove area of $A = 114\mu\text{m}^2$ and $K = 0.388\mu\text{m}$.

From a total of 17 layered implosion experiments, 7 shots were taken with ignition grade layers with $K < 0.7\mu\text{m}$ and 10 layers for tuning experiments, $0.7\mu\text{m} < K < 1.5\mu\text{m}$. Table I provides a summary of the experimental conditions and results of the layered implosion shots. The effect of non-perfect layers on the neutron yield has been estimated with radiation-hydrodynamic simulations that provides a yield factor, Y_F , from the K values and power spectral density value for the ice sphericity. The analysis shows for the 7 ignition grade layers $Y_F \geq 0.95$, and $0.6 < Y_F < 0.95$ for the remaining experiments.

III. LASER AND HOHLRAUM DRIVE

The layered capsule implosions are driven by gold hohlraums heated with 192 frequency-tripled (3ω) laser beams on the National Ignition Facility. The beams are arranged in four cones entering the hohlraum through the top and bottom LEHs; the inner two cones being at angles of 23.5° and 30° and the outer two cones being at 44.5° and 50° to the vertical axis.

Figure 3 shows examples of (a) the total 3ω laser powers used to drive cryogenic thermonuclear fuel implosions. These pulse shapes indicate the full range of power and energy variations in this study. The peak power varies from 300 TW to 430 TW and the total energy increases from (1.05 ± 0.02) MJ to (1.6 ± 0.03) MJ, respectively. Also shown in Fig. 3(b) are the power cone fraction for two experiments. We employ smoothed beams [18, 38–43] with polarization rotation [44, 45], smoothing by spectral dispersion with a laser bandwidth of 45 or 60 GHz and a 17 GHz frequency oscillator. In addition, continuous phase plates are employed that give elliptical vacuum spot sizes [46, 47] providing peak quad vacuum intensities of $I_{23.5} = 5.16 \times 10^{14}\text{W cm}^{-2}$, $I_{30} = 5.9 \times 10^{14}\text{W cm}^{-2}$, $I_{44.5} = 1.3 \times 10^{15}\text{W cm}^{-2}$, and $I_{50} = 1.4 \times 10^{15}\text{W cm}^{-2}$ for the 430 TW laser drive.

At these energies and powers, the hohlraum absorbs $80 - 90\%$ of the incident energy with the dominating loss mechanism being due to Stimulated Raman Scattering (SRS) [48, 49] on the inner cones of beams. At

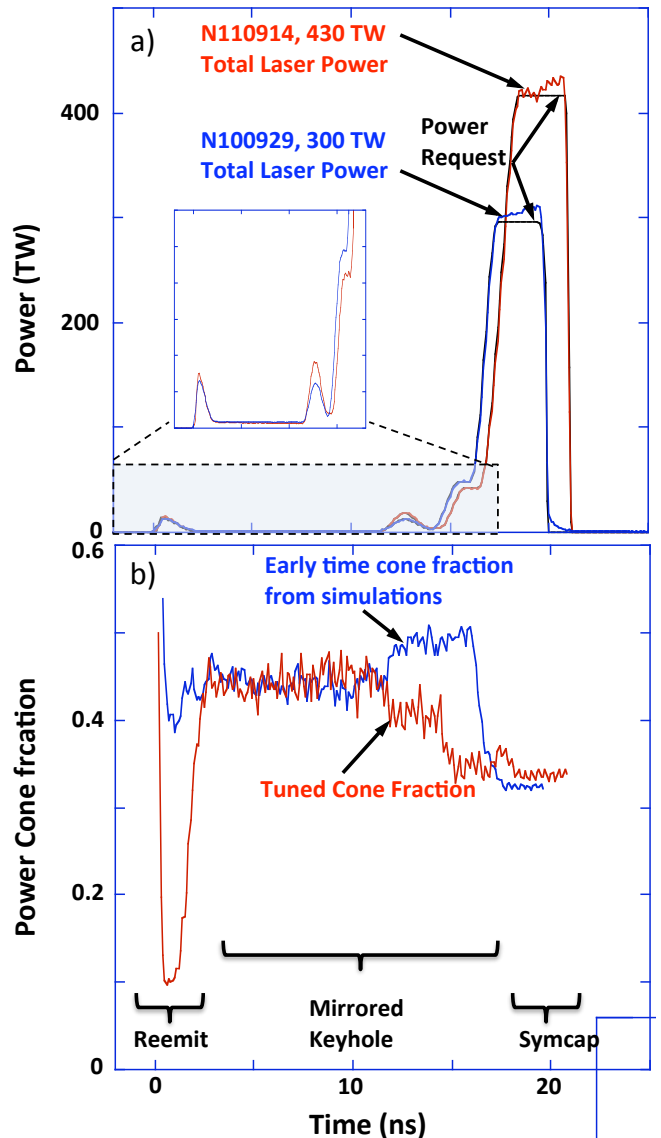


FIG. 3: (a) Examples of measured laser powers at a laser wavelength of 351 nm are shown for two hohlraum experiments with 1.6 MJ (shot N110914) and 1.05 MJ (shot N100929) drive. The inset shows the laser foot powers whose pickets have been tuned to achieve proper shock velocity and strength. (b) The laser power cone fraction, i.e., the inner (23.5° and 30°) cones of beam powers divided by the total laser power, is shown as a function of time. Three tuning platforms, the reemit, mirrored keyhole, and symcap experiments have been applied for tuning cone fraction and drive symmetry during the different parts of the drive.

our conditions, the SRS instability is saturated [43] as measured with a full aperture backscatter diagnostics and near backscatter imagers resulting in a total loss of (200 ± 40) kJ [50]. Scattering losses on the outer beams are below threshold for significant scattering [41, 42], a total of (210 ± 40) J of Stimulated Brillouin Scattering has been measured on a 50° quad of beams. While the SRS

power loss is compensated for by crossed beam power transfer as described in Sec. (IV), potential capsule fuel preheat from hot electrons [51, 52] has been shown to be small. Direct hard x-ray imaging of the capsule high-energy bremsstrahlung emission [25] has measured 500 J of electrons with energies > 170 keV that have the potential to generate fuel pre-heat; this value is about a factor of 2 below current estimated upper limits acceptable for ignition [1].

The hohlraum radiation temperature produced in these experiments is inferred from measurements of the x-ray power, P , in the energy range of $0 < E_{X-ray} < 20$ keV out of the LEH with the absolutely calibrated broadband x-ray spectrometer Dante [5, 28, 53, 54]. The measured radiant intensity provides the temperature via $dP/d\Omega = A_{LEH}(t)\phi(t)\cos\theta\sigma T_{RAD}^4/\pi$. Here, σ is the Stefan-Boltzmann constant and θ is the view angle of Dante towards the hohlraum axis. The dynamically varying source area, $A_{LEH}(t)$ is estimated from 3 – 5 keV x-ray images [55] of the LEH measured with the Static X-ray Imager. These measurements show a reduction of the LEH diameter to 83 % of the initial value. ϕ is the view factor that relates the Dante measured drive with the radiation temperature seen by the capsule.

Recent implementation of a time-integrating soft x-ray imager of the LEH at 900 eV has provided new measurements of the LEH aperture, indicating that about 10 % of the Dante measured radiant intensity is due to emission from the ablated Au plasma that reduces the LEH clear aperture [56]. Assuming 90 % of the measured signal is from emission of the hohlraum interior, applying the measured LEH aperture, and adding a small view-factor correction results in a 10 eV corrections for these experiments.

The internal hohlraum radiation temperatures are modeled by balancing the absorbed laser power with the x-ray power radiated into the wall, P_W , absorbed by the capsule, P_{CAP} , and the power that escapes though the LEH, P_{LEH} ,

$$\begin{aligned} & \eta_{CE} (P_L - P_{Backscatter}) \\ &= P_W + P_{LEH} + P_{CAP} \\ &= \sigma T_{RAD}^4 [(1 - \alpha_W)A_W + A_{LEH} + (1 - \alpha_{CAP})A_{CAP}] . \end{aligned} \quad (1)$$

With η_{CE} being the x-ray conversion efficiency from laser power to soft x-rays [57, 58]; α_W and α_{CAP} are the x-ray albedo of the hohlraum wall and the capsule, respectively. The albedo is defined as the ratio of re-emitted to incident x-rays. The hohlraum wall area, laser entrance hole area, and capsule surface area are denoted by A_W , A_{LEH} and A_{CAP} , respectively. Assuming a conversion efficiency of $\eta_{CE} = 0.9$ at peak laser power, Eq. (1) indicates peak radiation temperatures of 260 eV $< T_{RAD} < 305$ eV in good agreement with the results inferred from Dante measurements [15].

The solution of the rocket equation shows that achieving high radiation temperatures and low remaining mass [1] are important tuning parameters for obtaining high

capsule implosion velocities and for approaching ignition conditions.

$$V_{imp}(\text{km/s}) = 10^2(T_{RAD})^{\frac{1}{2}} \ln \frac{m_0}{m}, \quad (2)$$

with T_{RAD} in hundreds of eV or heV. Specifically, for the remaining mass we aim at $m/m_0 = 0.08$ with the expectation that this value results in tolerable ablator mix. Since the ignition threshold factor (ITF) that provides a quantitative estimate for the probability of ignition scales like V_{imp}^8 ([7]) increasing the implosion velocity to a point where additional margin can be achieved is an important ongoing area of effort.

In experiments that employ a 300 to 305 eV hohlraum radiation drive, we find that Si is a more efficient ablator than Ge indicating implosion velocities up to $V_{imp} = (350 \pm 20)$ km/s from radiography measurements [27, 31]. Here, the Si K-shell absorption edge at 2 keV provides the required M-band radiation pre-heat shielding of the fuel, but leads to a reduced dopant absorption of the thermal 300 eV hohlraum spectrum and to a reduced capsule albedo compared to experiments with a 1.3 keV L-edge of Ge, thus resulting in higher implosion velocities. Present velocities with the 430 TW, 1.6 MJ drive are 95 % of the ignition requirement of 370 km/s.

IV. IMPLOSION SYMMETRY

In this study, symmetry tuning has been performed throughout the whole duration of the laser pulse. In particular, SRS scattering losses on the inner beams have been compensated for and a symmetric radiation drive on the capsule has been achieved by taking advantage of crossed beam power transfer by laser scattering on self-generated plasma optics gratings in the LEH area [19, 20]. Specifically, the laser wavelengths of the 23.5° cones of beams and the 30° cones of beams have been tuned independently from the wavelength of the two outer cones of beams at 44.5° and 50° [62, 63]. The wavelength shift results in power transfer from the outer cones of laser beams to the two inner cones of beams and among the inner cones of beams. Power transfer increases the inner beam power by factors of 1.5 – 2 while allowing all beams to be operated with maximum laser power and producing the required symmetric soft x-ray drive on the capsule.

The crossed beam power transfer tuning mechanism takes advantage of the multiple laser beam interactions with the plasma in the LEH area where all the beams cross. The crossing lasers in the LEH produce spatial intensity modulations. These intensity modulations further drive plasma electron density modulations due to the ponderomotive force. If these modulations move with the plasma sound speed C_S (in the frame of the plasma) then modulations and laser scattering will grow to large levels and efficient energy transfer between beams will occur. In the rest frame, the power transfer rate, Q , is

determined by

$$Q \sim [(\omega_1 - \omega_2) - k_A (C_S - V_p) + i\nu]^{-2}. \quad (3)$$

In Eq. 3, V_p is the plasma flow velocity and ν is the Landau damping rate for acoustic fluctuations. The frequency de-tuning between pairs of beams is denoted as $\omega_1 - \omega_2$. This factor allows us to control the energy transfer between cones of beams in integrated hohlraum experiments, and the frequency difference can be set to transfer power in or out of the different cones of beams on NIF.

Symmetric DT implosions have been achieved by applying results from three different tuning platforms, the so-called symcap [19, 29], reemit [24], and mirrored key-hole [31] experiments. These three platforms set the laser cone fraction for various parts of the laser drive as indicated in Fig. 3(b).

First, symcap implosions have been used to tune the total laser wavelengths differences to optimize power transfer and symmetry during peak laser power where simple geometry considerations lead to a cone fraction close to 1/3 to operate all beams at maximum power. For examples of tuning results, see Refs. [15, 19, 21, 22, 29, 30, 62].

Second, reemit experiments are applied using a bismuth capsule that has a high albedo for 100 eV foot hohlraum radiation and whose 760 eV x-ray reemission during the first picket of the drive measures the radiation symmetry up to about $t = 2.5$ ns. Even during the early part of the laser pulse there is significant power transfer leading to a required cone fraction of 1/10, cf. Fig. 3(b).

Finally, while early experiments used calculations to determine the cone fraction during the remaining parts of the laser pulse, recently we have begun measuring the symmetry throughout the pulse using velocity interferometer measurements on the shock waves at two orthogonal angles [31, 64, 65]. Adjustments indicated in Fig. 3(b) during $12 \text{ ns} < t < 17 \text{ ns}$ are the result of this tuning platform.

Measurements of the implosion symmetry has been performed with equatorial and axial high-resolution ($10 \mu\text{m}$) pinhole imaging of the 9 keV x-ray emission from the central hot-spot plasma. Both temporally resolved (40 ps) data [5, 19, 22, 30] from gated microchannelplate detectors [66] and absolutely calibrated time-integrated image plate data in four broad band x-ray energy channels have been measured. The equatorial measurements can be quantified [67–69] by decomposing the soft x-ray flux asymmetry at the capsule into Legendre polynomials, P_n . Odd orders ($n = 1, 3, \dots$) are approximately zero due to the up-down illumination symmetry and low-order even modes ($n = 2, 4$) are the most important asymmetries. Higher order drive variations are negligibly small and smoothed by the hohlraum radiation environment.

In the axial direction, the implosion is characterized by azimuthal modes, M_n , that occur when coupling of the 23.5° and 30° cones of beams to the hohlraum is different [63]. In addition, the starburst observation holes that are cut in the hohlraum wall for characterizing the fuel

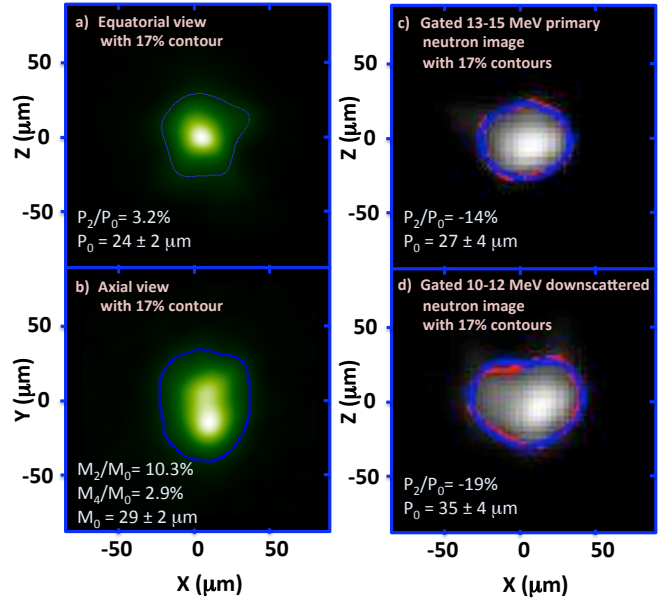


FIG. 4: Comparison of the x-ray emission images at 9-keV energy from the DT implosion shot N110914. Both, the (a) equatorial and (b) axial views are shown indicating symmetric conditions with P_2 close to zero and a residual M_2 mode. Also shown (c) is the primary (13-17 MeV) neutron image and (d) the down scattered (10-12 MeV) image. The analysis of the 17 % contours shows good symmetry and compression of 30 with a hot spot plasmas of $50 \mu\text{m}$ diameter close to the results from the x-ray emission measurements. The hohlraum cylindrical axis of symmetry is vertical.

layer may imprint an early azimuthal asymmetry before the holes close during the peak of the laser drive. Both effects will primarily produce M_4 modes.

Figure 4 shows the x-ray emission from the DT implosion with 1.6 MJ laser drive. These time-integrated 9 keV x-ray pinhole images show the following Legendre coefficients: $P_0 = 24 \mu\text{m}$, $P_2/P_0 = 0.032$, $P_4/P_0 = -0.026$. The orthogonal axial view also indicates a fairly symmetric implosion with $M_0 = 29 \mu\text{m}$, $M_2/M_0 = 0.103$, and $M_4/M_0 = 0.029$. These results compare well to the data from time-resolved x-ray images. For example, the gated data at x-ray bangtime at $t = 22.1 \pm 0.05$ ns show $M_0 = 23.2 \mu\text{m}$, $M_2/M_0 = 0.19$, and $M_4/M_0 = 0.037$. Figure 4(b) and the inset in Figure 5 compare time-integrated polar images with the results at bangtime for shot N110914.

We find that the x-ray emission measurements of hot spot shape approximately agree with the results from neutron imaging. This system observes the neutron signal from a scintillator with two gated CCD cameras that are timed to measure primary neutrons at 13-17 MeV or down scattered neutrons at 10-12 MeV. The image with energies of 13-17 MeV shows $P_0 = 27 \mu\text{m}$ and $P_2/P_0 = -0.014$. Two 17 % contour lines are shown, the red curves is from the raw data and the blue curve from

the best fit. The primary neutron image may be slightly larger than the x-ray emission image because it contains a small contribution from down scattered neutrons that are scattered in the dense fuel shell at larger radii. Here, the x-ray emission image is integrated over the x-ray emission time while the neutron image integrates over the nuclear burn duration. The x-ray framing camera measurements provide the x-ray emission duration of 120 ± 20 ps, which is close to simulations. While the nuclear measurements with γ -ray detectors [70] show a longer nuclear activity of 170 ± 30 ps. Also shown in Fig. 4 is the image of the down scattered neutrons that indicates a fairly symmetric implosion from the equatorial view providing a fuel shell with $P_0 = 35\mu\text{m}$ and $P_2/P_0 = -0.019$.

Figure 5 shows the measured fusion yield from layered DT implosions as a function of the measured M_4/M_0 values. Data are shown for the 1.4 MJ drive with one exception for the 1.6 MJ shot. Also shown are examples of polar x-ray images measured along the vertical axis of the hohlraum. The implosion with $M_4/M_0 = 0.13$ shows significant four-fold lobes at the location where the 30° cones of beams irradiate the hohlraum wall.

Calculations indicate that strong coupling of the 30° beams would produce an early compression of the capsule surface area that faces this part of the hohlraum wall (indicated as red arrows in the images of Fig. 5) leaving the remaining capsule surface that faces the 23.5° beams behind. Subsequently, being at larger radius the latter is absorbing more radiation and is consequently compressing to smaller radii. This phase reversal is indeed consistent with the experimental observations. By shifting the wavelength of the 23.5° cones of beams further to the red by an additional 1 to 2 Å at (1ω) , more power has been transferred to the 23.5° beams. In this case, we observe that a stronger drive from the 23.5° beams (indicated as green arrows in Fig. 5) results in stronger compression of the capsule surface area that faces the 30° beams.

By tuning the wavelength differences among the various cones we achieved M_4/M_0 values as small as 4 %, and a simultaneous increase in DT fusion yield by a factor of three. The most recent implosions where symmetry tuning with all three tuning platforms have been implemented have achieved symmetry values close the ignition requirements of 10 % for all modes and have resulted in the highest fusion yield, i.e., shot N111215. Nevertheless, the polar x-ray images indicate that future work is needed to achieve a fully symmetric implosion. These experiments will include a new tuning platform to measure M-modes during the foot of the drive by employing a polar reemit technique.

V. ENTROPY

The analytic solution [1, 4] for the burn fraction, Φ , shows that burning a significant fraction of DT fuel re-

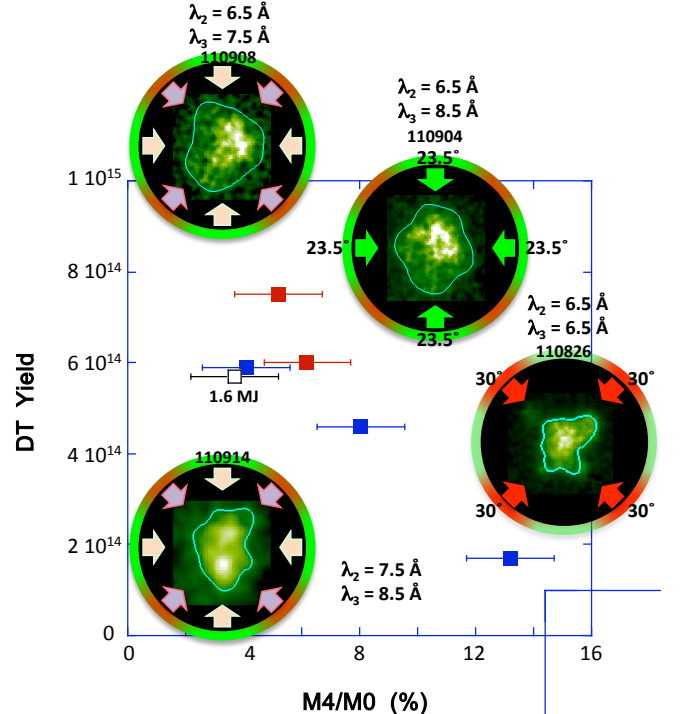


FIG. 5: DT fusion yield is shown as function of M_4/M_0 together with examples of polar x-ray images at peak emission time. Red and blue data points are for shots at 1.4 MJ, each set with the same laser pulse shape and cone fraction. The images correspond to the blue data. The black open symbol along with a polar x-ray image represent the 1.6 MJ drive with laser pulse shape and cone fraction consistent with the blue data points. Also shown are the wavelength separation λ_2 between the 30° cone and the outer cones of beams, and λ_3 between the 23.5° cone and the outer cones of beams. Larger separation results in larger power transfer.

quires areal densities of $\rho R > 1 \text{ g cm}^{-2}$

$$\Phi = \frac{\rho R}{\rho R + 6(\text{g cm}^{-2})}. \quad (4)$$

Figure 3(a) shows that the laser pulse contains four distinct intensity steps in time to compress the capsule with three distinct shocks, which are followed by quasi-adiabatic compression during the fourth peak. Also shown as inset are the laser powers during the foot indicating adjustments to the strength and timing of these shocks. These adjustments have been performed to produce a low adiabat implosion with $\alpha_{IF} < 1.5$ [16] (where the in-flight adiabat, α_{IF} is defined as the ratio of fuel pressure to Fermi degenerate pressure at the fuel density, $P = \alpha_{IF} P_F$ [1, 7, 71]). To achieve low values for α_{IF} , the shocks need to merge close to the inner DT solid fuel/gas interface. Significant deviations from the designed shock strength and/or timing leads to shock merger either within the ice layer or too far into the central gas region, which can lead to preheat and reduction

of the areal density at peak compression.

A series of shock tuning experiments [16, 23] that employs capsules filled with cryogenic liquid deuterium as a surrogate for cryogenic solid DT fuel has determined the adjustments to the pulse shape of order 10-20 %. This technique has been successfully established at the Omega laser at the University of Rochester [65] where experiments have led to the highest observed values of $\rho R = (0.295 \pm 0.044 \text{ g cm}^{-2})$ for directly driven implosion experiments [72, 73].

In the present experiments, the spatially averaged down scattered ratio (dsr) has been obtained using the Magnetic Recoil Spectrometer (MRS) [74] and three high-dynamic range Neutron Time Of Flight (NTOF) detectors, giving four different viewing angles to the imploded capsule. The MRS employs a CD foil (275 μm thick, 13 cm^2 area) at a distance of 26 cm from target chamber center. The DT neutrons from the implosion collide with the deuterons in the foil; the forward scattered deuterons are spectrally analyzed by a magnet at a distance of 570 cm from the foil. The DT neutrons transfer most of their momentum to the deuterons with $n(14.1 \text{ MeV}) + d \rightarrow n'(1.6 \text{ MeV}) + d(12.5 \text{ MeV})$. After passing the magnet, the recoil deuterons are measured with a series of CR-39 solid state nuclear track detectors and from their position allows inferring their energy spectrum and hence the neutron energy spectrum.

The NTOF array of photoconductive detectors and scintillator/photomultiplier systems at distances of 4.50 to 20 m measures the arrival time of the neutrons generated during the implosion. On NIF, six NTOF detectors measure the neutron spectrum as a function of neutron energy, integrated over the hot spot, which contains a distribution of temperature and burn rates. The thermal distribution results in a dispersion of the neutron arrival times at distant detectors [75] and allows extracting the relative ratio of down-scattered neutrons to the primary neutron signal [76].

The absolute neutron yield has also been measured with Nuclear Activation Diagnostics (NAD), where zirconium and copper undergo neutron reactions with energy thresholds just below the DT (Zr and Cu) neutron production energy region of interest. The radioactive decay of the reaction product provides the incident primary neutron fluence above the energy threshold. We find that the DT yield determined by these diagnostics are in excellent agreement with each other. The error bar for the absolute diagnostics, NAD and MRS are 7 % and 4 %, respectively. When comparing the results from all detectors we find for these experiments that the 14.1 MeV DT yield reaches 7.5×10^{14} with a standard variation of 2 %.

Figure 6 shows examples of MRS spectra for shots before and after shocks timing adjustments. The diagnostic setup was identical for the two shots, allowing a direct comparison of the deuteron spectra. The pre-tuning example, shot N110212 provided a dsr of 2.7 %. The post-tuning example, shot N110608 shows an increase by about a factor of 1.6 achieving a dsr of 4.3 %. The pri-

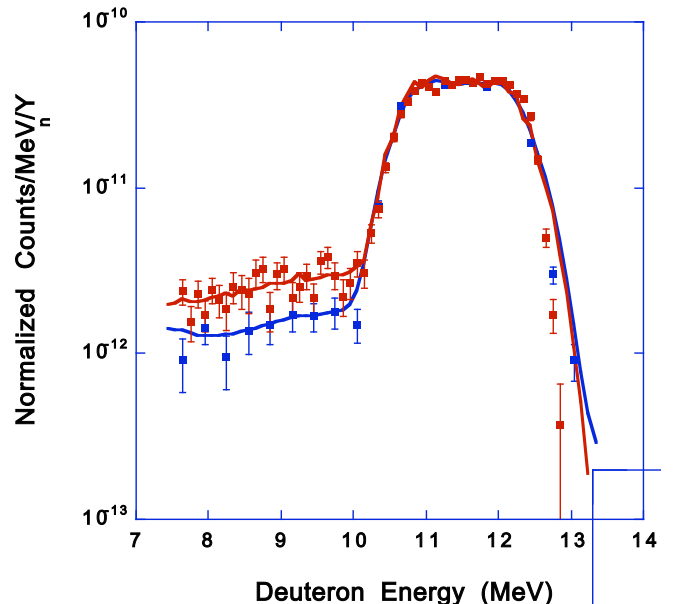


FIG. 6: Example of magnetic recoil spectrometer data from two experiments; N110212 (pre-shock timing blue points and best fit line) and N110608 (post-shock timing red points and best fit line). Data were taken with the same MRS foil thickness and normalized to 13-15 MeV neutron yield.

mary non-scattered neutrons produce the broad peak in the deuteron spectrum centered at 11.5 MeV, while the down-scattered neutrons are responsible for the deuteron signal between 7 and 10 MeV. The plots have been normalized by their 13-15 MeV neutron yields to show the increase in dsr. The increase of the dsr is also measured with the NTOF diagnostics albeit absolute values still differ by about 10-20 % likely reflecting spatial variations in areal density.

Table I summarizes the results for the areal densities as derived from the dsr measurements utilizing radiation hydrodynamic simulations, $\rho R [\text{g cm}^{-2}] = 21 \times \text{dsr}$. Areal densities have exceeded 1 g cm^{-2} when increasing the duration of the fourth pulse by 200 ps as delivered in a 1.6 MJ laser pulse to the hohlraum. The prolonged drive appears to assure that high areal densities prevail up to stagnation time; current values fulfill the requirement for burn fraction larger than 14 %, which is a pre-requisite for $\simeq 5 \text{ MJ}$ yield. Future experiments are planned to further improve shock timing to approach the predicted results for a tuned CH implosions, i.e., a dsr of 7 % and areal densities of 1.5 g cm^{-2} .

VI. IGNITION THRESHOLD FACTOR

To estimate performance and the scaling of layered implosion experiments to the ignition regime, we analyze neutron yield and dsr from x-ray and nuclear diagnostics, see Refs. [15] for a comprehensive description and

analysis of diagnostics results. The no burn DT yield, Y_n , and the dsr are combined in the ignition threshold factor; the $ITFx$ -value is defined as

$$ITFx = \left(\frac{Y_{DT}}{3.2 \times 10^{15}} \right) \left(\frac{dsr}{0.07} \right)^{2.3}. \quad (5)$$

This formalism allows the direct use of accurately measured quantities for estimating the proximity towards the ignition regime. A series of about 1000 two-dimensional simulations have shown that implosions with $ITFx$ values of about one show a 50 % probability for ignition and fusion yield.

To compare experiments with different deuterium fraction, we estimate a no burn DT equivalent yield. Generally, the observed 14.1 MeV neutron yield data follow a simple scaling that is derived from calculations of the total DT yield

$$Y_{DT} = f_D f_T n^2 \langle \sigma_{DT} v \rangle \times V \times \tau. \quad (6)$$

Here, $\langle \sigma_{DT} v \rangle$ is the DT fusion cross section averaged over the Maxwell Boltzmann velocity distribution function. f_D , f_T , and n are the fraction of deuterium and tritium in the plasma and the total atom number density, respectively. V is the hot spot volume and τ is the burn duration. The data show a $T^{4.7}$ -scaling (Table I and [15]) that is primarily a consequence of the cross section scaling with temperature. To compare experiments with different fraction of deuterium and to obtain the no burn DT equivalent yield, we scale the measured Y_n according to Eq. (6). For example, for a THD experiment with $f_D = 0.06$ and $f_T = 0.72$ the non burn DT equivalent yield is obtained by multiplying the measured yield with $(0.5^2)/(0.06 \times 0.72) \simeq 5.8$. Consequently, the use of small deuterium fractions in THD fuel allows experiments that approach $ITFx$ values of $\simeq 1$ without significant α -heating.

Figure 7 shows the DT equivalent yield versus the dsr from four campaigns; layered commissioning experiments are shown in black; post-shock timing shots with germanium doped CH ablaters are shown in blue; high velocity implosions with silicon doped CH ablaters are shown in red, and implosions with spherical shape tuning are shown in brown. Implosions with shock tuned pulses and with sufficient laser energy that avoids coasting produce the most improved dsr, the highest areal densities, and an $ITFx$ of 0.08. In addition, implosions with higher velocity as obtained with a 3.1 mm diameter LEH and with a fast laser rise in the fourth pulse have produced high yields at lower laser energy. In future experiments, these parameters will be optimized simultaneously to further improve implosion performance.

The implosion experiments were modeled [32] using the HYDRA 2D radiation-hydrodynamic code [77]. The x-ray source drive in the simulations was varied until it matched the shock velocity history observed [23] for the first 19 ns up to peak power and then matched the implosion trajectory measured via x-ray radiography [27].

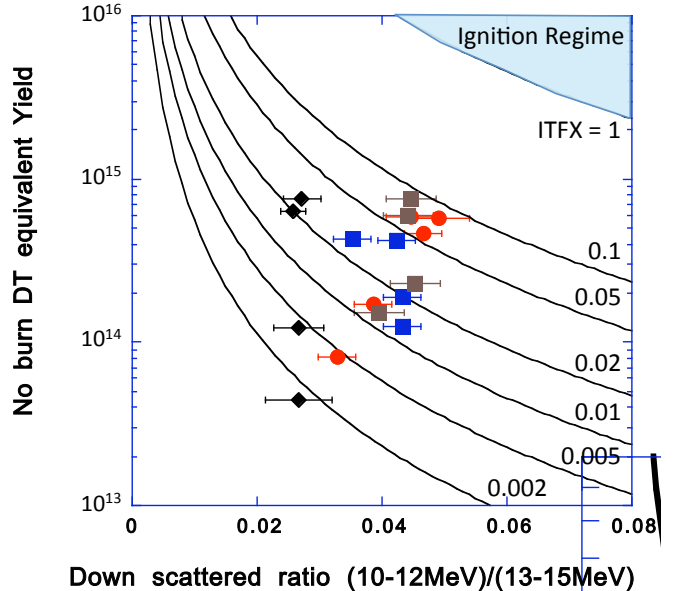


FIG. 7: The no burn DT equivalent fusion yield (i.e, without α -heating) versus the measured dsr has shown an increase by a factor of about 50 to about 0.08 in four experimental campaigns. Also shown are contours of equal $ITFx$, which increase from bottom left to top right as yield and DSR increase. Future campaign aim at further increasing both parameters to reach the ignition regime by approaching $ITFx = 1$ which indicates a 50 % probability for ignition for an implosion experiment.

The implosion symmetry was also matched using the plasma cross-beam transfer saturation parameter that determines the relative balance of inner and outer laser beam power [21].

Realistic levels of capsule ablator and ice surface roughness were included for modes up to 60, since these are predicted by the point design to have the highest Rayleigh-Taylor (RT) instability growth rate [7]. When capsule and ice roughness has been applied to all the surfaces and interfaces in the calculation, significant RT growth was seen at the ice: gas interface compared to 2D clean calculations, cooling the hotspot, lowering neutron yield and areal density. These simulations include corrections to the drive caused by deviations from requested to actual laser pulse shapes, variations in target dimensions, and yield factors due to ice grooves.

The results of the simulations without deposition of α particles, i.e. no α heating, are also listed in Table I. Generally, the dsr from the mode 60 simulations for the shock-tuned implosions are within 25 % of the measurements while the simulated adiabat inferred is $1.5 < \alpha_{IF} < 1.73$. In addition, with one exception the simulations match the observed ion temperature to within 15 %.

Significant discrepancies are observed in the measured DT yields, which are observed to be of order 10 % of the

calculated values. This observed discrepancy in DT yield can also be seen in estimates using Eq. (6) with measured values for temperature, density, volume and burn duration. Here, the ion temperatures are the weighted mean of the measured ion temperatures from NTOF with a typical standard variation and error bar of 0.1 keV. The low yield is explained by lower than calculated hot spot mass, which could be a consequence of mix. Upcoming experiments on NIF are aimed to optimize the velocity-mix trade off and to improve the hydrodynamic stability of the implosion.

VII. PRESSURE

It has been shown in Refs. [12, 14] that the volume-averaged pressures and confinement time of ICF plasmas can be tied to a generalized Lawson criterion that indicates the proximity of a fusion experiment towards the ignition regime. By fitting x-ray images, burn width, neutron time-of-flight ion temperature, yield, and fuel ρR , a nearly unique constraints on conditions can be obtained to model hot spot and fuel conditions that are entirely consistent with the observables. This model [78] has been used to determine hot spot density, pressure, areal density, and total energy, not available from any single diagnostic. Since the pressure in ICF targets at stagnation is designed to be approximately isobaric, uncertainties in these quantities may be estimated by comparing results derived from conditions in the hot spot with those in the fuel.

For the hot spot plasma, temperature and density measurements have been performed with high energy x-ray emission data. For this purpose, absolutely measured high-energy x-ray images have been analyzed using calculations of time-integrated bremsstrahlung power, P_B . The images consist of a 11 – 20 keV channel from a Ross pair with $7\mu\text{m}$ Mo + $1525\mu\text{m}$ Kapton paired with $24\mu\text{m}$ Ge coated on $200\mu\text{m}$ graphite + $1525\mu\text{m}$ Kapton, and a higher energy channel at 20 – 60 keV from a set with a $2525\mu\text{m}$ Kapton filter paired with $7\mu\text{m}$ Mo + $1525\mu\text{m}$ Kapton. At such high x-ray energies, calculations indicate that the signal is not significantly affected by absorption in the shell and the bremsstrahlung analysis provides $n_e = 8 \times 10^{24}\text{cm}^{-3}$ for shot N110914. Here, we utilized $T_i = 3.6$ keV from NTOF and assumed $T_e = T_i$ at these high densities. This results in an estimated stagnation pressure of $P = 92$ Gbar, which represents a significant increase from the first layered experiment that showed pressures of 9 Gbar at 1.05 MJ.

The hot spot pressure values compare with estimates of the fuel pressure. Using $\rho R = 1 \text{ g cm}^{-2}$ inferred from MRS data and using an upper estimate for the shell thickness of $\Delta r = 17\mu\text{m}$ provides a shell density of $\rho \simeq 600 \text{ g cm}^{-3}$ and electron density of $n_e = \rho/(2.5m_p) = 1.4 \times 10^{26} \text{ cm}^{-3}$. Assuming close to Fermi degenerate conditions and estimating the Fermi degenerate pressure $P_F = 2.17 \times 10^{12}[(\text{erg/g})/(\text{g/cm}^{-3})]\rho^{2/3}$

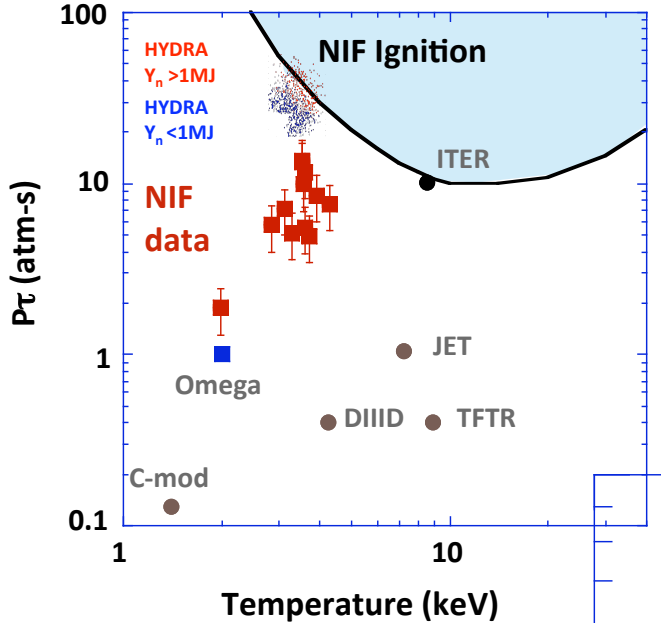


FIG. 8: Generalized Lawson confinement parameter, averaged pressure times confinement time, $P\tau$, versus the ion temperature is shown. The figure compares finding from NIF implosions, the HYDRA data base, Omega laser data, and various tokamak results. The calculations indicate that ignition will require a factor of three higher values for $P\tau$ with pressures above 300 Gbar.

and using $P = \alpha_{IF}P_F$, we arrive at $P_F = 90$ Gbar and $P = 135$ Gbar.

These values must be compared with the model pressure from the best fit of all experimental observables

$$P = 116 \text{ Gbar} \quad (7)$$

and using $\tau = 100$ ps as a lower burn width estimate

$$P\tau = 11.4 \text{ atm s.} \quad (8)$$

This comparison indicates that the error bar of $P\tau$ can be estimated as $\pm 30\%$. In this estimate, the error in the burn width measurements τ largely cancels; using for example larger values for τ will result in reduced inferred values for P .

Figure 7 shows the pressure-time product versus the measured ion temperature for NIF implosion shots, cf. Table I. The data show an increase in performance reaching values within a factor of three required for ignition. The highest data points with $P\tau > 10 \text{ atm s}$ are from shots N110914 and N111215. The results of the radiation-hydrodynamic HYDRA modeling indicate that ignition conditions will be reached at $P\tau \simeq 30$ and no-burn temperatures of $T = 4$ keV. This temperature is obtained from radiation-hydrodynamic simulations and is close, but slightly below the so-called ideal ignition temperature of 4.3 keV when alpha heating power is exceeding bremsstrahlung losses in an optically thin plasma. The former is obtained by equating

bremsstrahlung losses with Eq. 6 that is multiplied by the alpha particle energy. The slightly lower temperatures needed in simulations indicates that radiation losses are reduced due to high shell opacities. The simulations with and without alpha particle deposition (i.e., for highly diluted THD and DT fuel) show that ignition and fusion burn with > 1 MJ yield will occur for these pressures and temperatures.

In ICF implosions, the required $P\tau$ values for ignition are no burn numbers which define a threshold for an explosive growth of yield. Thus, post ignition pressures and temperatures are very different from pre-ignition numbers. Larger ICF capsules that are designed for high-gain fusion experiments [79, 80] use about an order of magnitude more fuel, but overall the $P\tau$ conditions are not be very different.

The NIF values well exceed data from previous fusion experiments [12] including Omega [72, 73] and magnetic confinement fusion plasmas that are of order 1 atm \times s in both cases. For JET, the core ion temperature reached 28 keV at a density of $3.3 \times 10^{13} \text{ cm}^{-3}$ and confinement about 0.9 s. Quoted central total pressure (all species) is about 0.35 MPa [81, 82] while averaged pressure about a factor of three lower as indicated in the figure. DIII-D reached a core performance of temperatures of 18.1 keV and densities of $8.5 \times 10^{13} \text{ cm}^{-3}$ for ions in the central region. Quoted central pressure (total across all species) is 0.33 MPa with averaged data points approximately a factor of three lower. Confinement time was 0.4 s [83, 84]. In Fig. 7 averaged pressure and temperature data are shown; note that for tokamak data points with $T_i > T_e$ the ignition curve will move up. Other data points are adopted from Ref. [12].

VIII. CONCLUSIONS AND OUTLOOK

Present indirect drive inertial confinement fusion experiments on the National Ignition Facility show that

ICF implosions with the highest areal densities and neutron yields achieved on laser facilities to date. This achievement is the result of the first hohlraum and capsule tuning experiments where the stagnation pressures have been systematically increased by more than a factor of 10 by fielding low-entropy implosions through the control of radiation symmetry, small hot electron production, and proper shock timing. The stagnation pressure is above 100 Gbar resulting in high Lawson confinement parameters of $P\tau \simeq 10$ atm s. Comparisons with radiation-hydrodynamic simulations indicate that the pressure is within a factor of three required for reaching ignition and high yield.

We expect that the 1-D performance of our implosions will soon meet or exceed the ignition implosion velocity providing margin for future optimization in areas of mix and pressure. Future experiments will use depleted uranium hohlraums [31] where recent experiments have been observed to provide reduced hohlraum wall losses due to improved opacity at low heat capacity. These improvements along with optimized hohlraum geometry and laser power will be fielded for future tuning experiments with the goal to reach values of 30 atm s, which are predicted for the ignition regime.

Acknowledgements

This work performed under the auspices of the U.S. Department of Energy by Lawrence Livermore National Laboratory under Contract DE-AC52-07NA27344. This work was also supported by the U.S. Department of Energy Office of Inertial Confinement Fusion under Cooperative Agreement No. DE-FC52-08NA28302.

-
- [1] J. D. Lindl, Phys. Plasmas **2**, 3933 (1995).
 - [2] J. D. Lindl, P. Amendt, R. L. Berger, S. G. Glendinning, S. H. Glenzer, S. W. Haan, R. L. Kauffman, O. L. Landen, and L. J. Suter, Phys. Plasmas **11**, 339 (2004).
 - [3] S. W. Haan, S. M. Pollaine, J. D. Lindl, L. J. Suter, R. L. Berger, L. V. Powers, W. E. Alley, P. A. Amendt, J. A. Futterman, W. K. Levedahl, M. D. Rosen, D. P. Rowley, R. A. Sacks, A. I. Shestakov, G. L. Strobel, M. Tabak, S. V. Weber, G. B. Zimmerman, W. J. Krauser, D. C. Wilson, S. V. Coggeshall, D. B. Harris, N. M. Hoffman, B. H. Wilde, Phys. Plasmas, **2**, 2480 (1995).
 - [4] Atzeni S, Meyer-ter-Vehn J, The Physics of Inertial Fusion (Oxford Univ. Press, New York, 2004)
 - [5] S. H. Glenzer, B. J. MacGowan, N. B. Meezan, P. A. Adams, J. B. Alfonso, E. T. Alger, Z. Alherz, L. F. Alvarez, S. S. Alvarez, P. V. Amick, K. S. Andersson, S. D. Andrews, G. J. Antonini, P. A. Arnold, D. P. Atkin-
 - son, L. Auyang, S. G. Azevedo, B. N. M. Balaoring, J. A. Baltz, F. Barbosa, G. W. Bardsley, D. A. Barker, A. I. Barnes, A. Baron, R. G. Beeler, B. V. Beeman, L. R. Belk, J. C. Bell, P. M. Bell, R. L. Berger, M. A. Bergonia, L. J. Bernardez, L. V. Berzins, R. C. Bettenhausen, L. Bezerides, S. D. Bhandarkar, C. L. Bishop, E. J. Bond, D. R. Bopp, J. A. Borgman, J. R. Bower, G. A. Bowers, M. W. Bowers, D. T. Boyle, D. K. Bradley, J. L. Bragg, J. Braucht, D. L. Brinkerhoff, D. F. Browning, G. K. Brunton, S. C. Burkhardt, S. R. Burns, K. E. Burns, B. Burr, L. M. Burrows, R. K. Butlin, N. J. Cahayag, D. A. Callahan, P. S. Cardinale, R. W. Carey, J. W. Carlson, A. D. Casey, C. Castro, J. R. Celeste, A. Y. Chakicherla, F. W. Chambers, C. Chan, H. Chandrasekaran, C. Chang, R. F. Chapman, K. Charron, Y. Chen, M. J. Christensen, A. J. Churdy, T. J. Clancy, B. D. Cline, L. C. Clowdus, D. G. Cocherell, F. E. Cofeld, S. J. Cohen,

- R. L. Costa, J. R. Cox, G. M. Curnow, M. J. Dailey, P. M. Danforth, R. Darbee, P. S. Datte, J. A. Davis, G. A. Deis, R. D. Demaret, E. L. Dewald, P. Di Nicola, J. M. Di Nicola, L. Divol, S. Dixit, D. B. Dobson, T. Döppner, J. D. Driscoll, J. Dugorepec, J. J. Duncan, P. C. Dupuy, E. G. Dzenitis, M. J. Eckart, S. L. Edson, G. J. Edwards, M. J. Edwards, O. D. Edwards, P. W. Edwards, J. C. Ellefson, C. H. Ellerbee, G. V. Erbert, C. M. Estes, W. J. Fabyan, R. N. Fallejo, M. Fedorov, B. Felker, J. T. Fink, M. D. Finney, L. F. Finnie, M. J. Fischer, J. M. Fisher, B. T. Fishler, J. W. Florio, A. Forsman, C. B. Foxworth, R. M. Franks, T. Frazier, G. Frieder, T. Fung, G. N. Gawinski, C. R. Gibson, E. Giraldez, S. M. Glenn, B. P. Golick, H. Gonzales, S. A. Gonzales, M. J. Gonzalez, K. L. Grifn, J. Grippen, S. M. Gross, P. H. Gschweng, G. Gururangan, K. Gu, S. W. Haan, S. R. Hahn, B. J. Haid, J. E. Hamblen, B. A. Hammel, A. V. Hamza, D. L. Hardy, D. R. Hart, R. G. Hartley, C. A. Haynam, G. M. Heestand, M. R. Hermann, G. L. Hermes, D. S. Hey, R. L. Hibbard, D. G. Hicks, D. E. Hinkel, D. L. Hippel, J. D. Hitchcock, D. L. Hodtwalker, J. P. Holder, J. D. Hollis, G. M. Holtmeier, S. R. Huber, A. W. Huey, D. N. Hulsey, S. L. Hunter, T. R. Huppler, M. S. Hutton, N. Izumi, J. L. Jackson, M. A. Jackson, K. S. Jancaitis, D. R. Jedlovec, B. Johnson, M. C. Johnson, T. Johnson, M. P. Johnston, O. S. Jones, D. H. Kalantar, J. H. Kamperschroer, R. L. Kauffman, G. A. Keating, L. M. Kegelmeyer, S. L. Kenitzer, J. R. Kimbrough, K. King, R. K. Kirkwood, J. L. Klingmann, K. M. Knittel, T. R. Kohut, K. G. Koka, S. W. Kramer, J. E. Krammen, K. G. Krauter, G. W. Krauter, E. K. Krieger, J. J. Kroll, K. N. La Fortune, L. J. Lagin, V. K. Lakamsani, O. L. Landen, S. W. Lane, A. B. Langdon, S. H. Langer, N. Lao, D. W. Larson, D. Latray, G. T. Lau, S. Le Pape, B. L. Lechleiter, Y. Lee, T. L. Lee, J. Li, J. A. Liebman, J. D. Lindl, S. F. Locke, H. K. Loey, R. A. London, F. J. Lopez, D. M. Lord, R. R. Lowe-Webb, J. G. Lown, A. P. Ludwigsen, N. W. Lum, R. R. Lyons, T. Ma, A. J. MacKinnon, M. D. Magat, D. T. Maloy, T. N. Malsbury, G. Markham, R. M. Marquez, A. A. Marsh, C. D. Marshall, S. R. Marshall, I. L. Maslenikov, D. G. Mathisen, G. J. Mauger, M. -Y. Mauvais, J. A. McBride, T. McCarville, J. B. McCloud, A. McGrew, B. McHale, A. G. MacPhee, J. F. Meeker, J. S. Merrill, E. P. Mertens, P. A. Michel, M. G. Miller, T. Mills, J. L. Milovich, R. Miramontes, R. C. Montesanti, M. M. Montoya, J. Moody, J. D. Moody, K. A. Moreno, J. Morris, K. M. Morris-ton, J. R. Nelson, M. Neto, J. D. Neumann, E. Ng, Q. M. Ngo, B. L. Olejniczak, R. E. Olson, N. L. Orsi, M. W. Owens, E. H. Padilla, T. M. Pannell, T. G. Parham, R. W. Patterson, Jr., G. Pavel, R. R. Prasad, D. Pendleton, F. A. Penko, B. L. Pepmeier, D. E. Petersen, T. W. Phillips, D. Pigg, K. W. Piston, K. D. Pletcher, C. L. Powell, H. B. Radousky, B. S. Raimondi, J. E. Ralph, R. L. Rampke, R. K. Reed, W. A. Reid, V. V. Rekow, J. L. Reynolds, J. J. Rhodes, M. J. Richardson, R. J. Rinnert, B. P. Riordan, A. S. Rivenes, A. T. Rivera, C. J. Roberts, J. A. Robinson, R. B. Robinson, S. R. Robison, O. R. Rodriguez, S. P. Rogers, M. D. Rosen, G. F. Ross, M. Runkel, A. S. Runtal, R. A. Sacks, S. F. Sailors, J. T. Salmon, J. D. Salmonson, R. L. Saunders, J. R. Schaffer, T. M. Schindler, M. J. Schmitt, M. B. Schneider, K. S. Segraves, M. J. Shaw, M. E. Sheldrick, R. T. Shelton, M. K. Shielt, S. J. Shiromizu, M. Shor, L. L. Silva, S. A. Silva, K. M. Skulina, D. A. Smauley, B. E. Smith, L. K. Smith, A. L. Solomon, S. Sommer, J. G. Soto, N. I. Spafford, D. E. Speck, P. T. Springer, M. Stadermann, F. Stanley, T. G. Stone, E. A. Stout, P. L. Stratton, R. J. Strausser, L. J. Suter, W. Sweet, M. F. Swisher, J. D. Tappero, J. B. Tassano, J. S. Taylor, E. A. Tekle, C. Thai, C. A. Thomas, A. Thomas, A. L. Throop, G. L. Tietbohl, J. M. Tillman, R. P. J. Town, S. L. Townsend, K. L. Tribbey, D. Trummer, J. Truong, J. Vaher, M. Valadez, P. Van Arsdall, A. J. Van Prooyen, E. O. Vergel de Dios, M. D. Vergino, S. P. Vernon, J. L. Vickers, G. T. Villanueva, M. A. Vitalich, S. A. Vonhof, F. E. Wade, R. J. Wallace, C. T. Warren, A. L. Warrick, J. Watkins, S. Weaver, P. J. Wegner, M. A. Weingart, J. Wen, K. S. White, P. K. Whitman, K. Widmann, C. C. Widmayer, K. Wilhelmsen, E. A. Williams, W. H. Williams, L. Willis, E. F. Wilson, B. A. Wilson, M. C. Witte, K. Work, P. S. Yang, B. K. Young, K. P. Youngblood, R. A. Zacharias, T. Zaleski, P. G. Zapata, H. Zhang, J. S. Zielinski, J. L. Kline, G. A. Kyrala, C. Niemann, J. D. Kilkenny, A. Nikroo, B. M. Van Wontghem, L. J. Atherton, and E. I. Moses, Phys. Rev. Lett. **106**, 085004 (2011).
- [6] O. L. Landen, J. Edwards, S. W. Haan, H. F. Robey, J. Milovich, B. K. Spears, S. V. Weber, D. S. Clark, J. D. Lindl, B. J. MacGowan, E. I. Moses, J. Atherton, P. A. Amendt, T. R. Boehly, D. K. Bradley, D. G. Braun, D. A. Callahan, P. M. Celliers, G. W. Collins, E. L. Dewald, L. Divol, J. A. Frenje, S. H. Glenzer, A. Hamza, B. A. Hammel, D. G. Hicks, N. Hoffman, N. Izumi, O. S. Jones, J. D. Kilkenny, R. K. Kirkwood, J. L. Kline, G. A. Kyrala, M. M. Marinak, N. Meezan, D. D. Meyerhofer, P. Michel, D. H. Munro, R. E. Olson, A. Nikroo, S. P. Regan, L. J. Suter, C. A. Thomas and D. C. Wilson, 2011 Phys. Plasmas **18** 051002 (2011).
- [7] S. W. Haan, J. D. Lindl, D. A. Callahan, D. S. Clark, J. D. Salmonson, B. A. Hammel, L. J. Atherton, R. C. Cook, M. J. Edwards, S. Glenzer, A. V. Hamza, S. P. Hatchett, M. C. Herrmann, D. E. Hinkel, D. D. Ho, H. Huang, O. S. Jones, J. Kline, G. Kyrala, O. L. Landen, B. J. MacGowan, M. M. Marinak, D. D. Meyerhofer, J. L. Milovich, K. A. Moreno, E. I. Moses, D. H. Munro, A. Nikroo, R. E. Olson, K. Peterson, S. M. Pollaine, J. E. Ralph, H. F. Robey, B. K. Spears, P. T. Springer, L. J. Suter, C. A. Thomas, R. P. Town, R. Vesey, S. V. Weber, H. L. Wilkins, D. C. Wilson, Phys. Plasmas **18** 051001 (2011).
- [8] M. J. Edwards, J. D. Lindl, B. K. Spears, S. V. Weber, L. J. Atherton, D. L. Bleuel, D. K. Bradley, D. A. Callahan, C. J. Cerjan, D. Clark, G. W. Collins, J. E. Fair, R. J. Fortner, S. H. Glenzer, S. W. Haan, B. A. Hammel, A. V. Hamza, S. P. Hatchett, N. Izumi, B. Jacoby, O. S. Jones, J. A. Koch, B. J. Kozioziemski, O. L. Landen, R. Lerche, B. J. MacGowan, A. J. MacKinnon, E. R. Mapoles, M. M. Marinak, M. Moran, E. I. Moses, D. H. Munro, D. H. Schneider, S. M. Sepke, D. A. Shaughnessy, P. T. Springer, R. Tommasini, L. Bernstein, W. Stoeffl, R. Betti, T. R. Boehly, T. C. Sangster, V. Yu. Glebov, P. W. McKenty, S. P. Regan, D. H. Edgell, J. P. Knauer, C. Stoeckl, D. R. Harding, S. Batha, G. Grim, H. W. Herrmann, G. Kyrala, M. Wilke, D. C. Wilson, J. Frenje, R. Petrasso, K. Moreno, H. Huang, K. C. Chen, E. Giraldez, J. D. Kilkenny, M. Mauldin, N. Hein, M. Hoppe, A. Nikroo, and R. J. Leeper, Phys. Plasmas **18**

- 051003 (2011).
- [9] J. D. Lawson, Proceedings of the Physical Society B, **70**, p. 6 (1957).
- [10] C. D. Zhou and R. Betti Phys. Plasmas **15**, 102707, (2008)
- [11] C. D. Zhou and R. Betti, Phys. Plasmas **16**, 079905 (2009).
- [12] R. Betti, P. Y. Chang, B. K. Spears, K. S. Anderson, J. Edwards, M. Fatenejad, J. D. Lindl, R. L. McCrory, R. Nora, and D. Shvarts, Phys. Plasmas **17**, 058102 (2010).
- [13] Py. Chang, R. Betti, B. K. Spears, K. S. Anderson, J. Edwards, M. Fatenejad, J. D. Lindl, R. L. McCrory, R. Nora, and D. Shvarts, Phys. Rev. Letters **104** 035002 (2010).
- [14] B. K. Spears, Phys. Plasmas **19**, (2012) *submitted*
- [15] S. H. Glenzer, Plasma Phys. Cont. Fusion (2012) *to be published*.
- [16] A. J. MacKinnon, Physics Review Letters (2012) *submitted*.
- [17] E. I. Moses and C. R. Wuest, Fusion Sci. Tech. **47**, 314 (2005).
- [18] C. Haynam, J. M. Auerbach, M. W. Bowers, S. N. Dixit, G. V. Ebert, G. M. Heestand, M. A. Henesian, M. R. Hermann, K. S. Jancaitis, K. R. Manes, C. D. Marshall, N. C. Metha, J. Menapace, E. Moses, J. R. Murray, M. C. Nostrand, C. D. Orth, R. Patterson, R. A. Sacks, M. J. Shaw, M. Spaeth, S. B. Sutton, W. H. Williams, C. C. Widmayer, R. K. White, S. T. Yang, B. M. Van Wonterghem , Appl. Optics **46**, 3276 (2007).
- [19] S. H. Glenzer, B. J. MacGowan, P. Michel, N. B. Meezan, L. J. Suter, S. N. Dixit, J. L. Kline, G. A. Kyrala, D. K. Bradley, D. A. Callahan, E. L. Dewald, L. Divol, E. Dzenitis, M. J. Edwards, A. V. Hamza, C. A. Haynam, D. E. Hinkel, D. H. Kalantar, J. D. Kilkenny, O. L. Landen, J. D. Lindl, S. LePape, J. D. Moody, A. Nikroo, T. Parham, M. B. Schneider, R. P. J. Town, P. Wegner, K. Widmann, P. Whitman, B. K. F. Young, B. Van Wonterghem, L. J. Atherton, E. I. Moses, Science **327**, 1228 (2010).
- [20] P. Michel, L. Divol, E. A. Williams, Weber, C. A. Thomas, D. A. Callahan, S. W. Haan, J. D. Salmonson, S. Dixit, D. E. Hinkel, M. J. Edwards, B. J. MacGowan, J. D. Lindl, S. H. Glenzer, L. J. Suter, Phys. Rev. Lett. **102**, 025004 (2009).
- [21] P. Michel, S. H. Glenzer, L. Divol, D. K. Bradley, D. Callahan, S. Dixit, S. Glenn, D. Hinkel, R. K. Kirkwood, J. L. Kline, W. L. Kruer, G. A. Kyrala, S. LePape, N. B. Meezan, R. Town, K. Widmann, E. A. Williams, B. J. MacGowan, J. Lindl, L. J. Suter, Phys. Plasmas **17** 056305 (2010).
- [22] R. P. J. Town, M. D. Rosen, P. A. Michel, L. Divol, J. D. Moody, G. A. Kyrala, M. B. Schneider, J. L. Kline, C. A. Thomas, J. L. Milovich, D. A. Callahan, N. B. Meezan, D. E. Hinkel, E. A. Williams, R. L. Berger, M. J. Edwards, L. J. Suter, S. W. Haan, J. D. Lindl, E. L. Dewald, S. Dixit, S. H. Glenzer, O. L. Landen, E. I. Moses, H. A. Scott, J. A. Harte, G. B. Zimmerman, Phys. Plasmas **18** 056302 (2011).
- [23] H. F. Robey, Phys. Plasmas (2012), *to be published*.
- [24] E. L. Dewald, J. Milovich, C. Thomas, J. Kline, C. Sorce, S. Glenn, and O. L. Landen, Phys. Plasmas **18**, 092703 (2011).
- [25] T. Döppner, Physics Review Letters (2012) *submitted*.
- [26] S. Regan, Physics Review Letters (2012) *submitted*.
- [27] D. G. Hicks, B. K. Spears, D. G. Braun, R. E. Olson, C. M. Sorce, P. M. Celliers, G. W. Collins, and O. L. Landen, Phys of Plasmas, bf 17, 102703, (2010).
- [28] J. L. Kline, S. H. Glenzer, R. E. Olsen, L. J. Suter, K. Widmann, D. A. Callahan, S. N. Dixit, C. A. Thomas, D. E. Hinkel, E. A. Williams, A. S. Moore, J. Celeste, E. Dewald, W.W. Hsing, A. Warrick, J. Atherton, S. Azevedo, R. Beeler, R. Berger, A. Conder, L. Divol, C. A. Haynam, D. H. Kalantar, R. Kauffman, G. A. Kyrala, J. Kilkenny, J. Lieberman, S. Le Pape, D. Larson, N. B. Meezan, P. Michel, J. Moody, M. D. Rosen, M. B. Schneider, B. Van Wonterghem, R. J. Wallace, B. K. Young, O. L. Landen, and B. J. MacGowan, Phys. Rev. Lett. **106**, 085003 (2011).
- [29] N. B. Meezan, J. L. Atherton, D. A. Callahan, E. L. Dewald, S. Dixit, E. G. Dzenitis, M. J. Edwards, C. A. Haynam, D. E. Hinkel, O. S. Jones, O. Landen, R. A. London, P. A. Michel, J. D. Moody, J. L. Milovich, M. B. Schneider, C. A. Thomas, R. P. J. Town, A. L. Warrick, S. V. Weber, K. Widmann, S. H. Glenzer, L. J. Suter, B. J. MacGowan, J. L. Kline, G. A. Kyrala, and A. Nikroo, Phys. Plasmas **17** 056304 (2010).
- [30] G. A. Kyrala, J. L. Kline, S. Dixit, S. Glenzer, D. Kalantar, D. Bradley, N. Izumi, N. Meezan, O. Landen, D. Callahan, S. V. Weber, J. P. Holder, S. Glenn, M. J. Edwards, J. Koch, L. J. Suter, S. Haan, R. P. J. Town, P. Michel, O. Jones, S. Langer, J. D. Moody, E. L. Dewald, T. Ma, J. Ralph, A. Hamza, and E. Dzenitis, Phys. Plasmas **18** 056307 (2011).
- [31] D. A. Callahan, Phys. Plasmas (2012) *submitted*.
- [32] O. S. Jones, Phys. Plasmas (2012) *submitted*.
- [33] Kucheyev S O and Hamza A V 2010, J. Appl. Physics **108**, 091101
- [34] J. R. Miller, Los Alamos Scientific Laboratory Report LA-6245-PR, p. 82 (1975); Methods and Apparatus for Producing Cryogenic Inertially Driven Fusion Targets, U. S. Patent 4,292,340 (Jan. 1987).
- [35] A. J. Martin, R. J. Simms, and D. L. Musinski, Sci. Technol. A **6**, 1885 (1988).
- [36] J. K. Hoffer and L. R. Foreman, Phys. Rev. Lett. **60**, 1310 (1988).
- [37] B. J. Kozioziemski, J. A. Koch, A. Barty, H. E. Martz, W. K. Lee, K. Fezzaa, J. Appl. Phys. **97**, 063103 (2005).
- [38] B. J. MacGowan, B. B. Afeyan, C. A. Back , R. L. Berger, G. Bonnaud, M. Casanova, B. I. Cohen, D. E. Desenne, D. F. DuBois, A. Dulieu, K. G. Estabrook, J. C. Fernandez, S. H. Glenzer, D. E. Hinkel, T. B. Kaiser, D. H. Kalantar, R. L. Kauffman, R. K. Kirkwood, W. L. Kruer, A. B. Langdon, B. F. Lasinski, D. S. Montgomery, J. D. Moody, D. H. Munro, L. V. Powers, H. A. Rose, C. Rousseaux, R. E. Turner, B. H. Wilde, S. C. Wilks, and E. A. Williams, Phys. Plasmas **3** 2029 (1995).
- [39] S. H. Glenzer, D. H. Froula, L. Divol, M. Dorr, R. L. Berger, S. Dixit, B. A. Hammel, C. Haynam, J. A. Hittinger, J. P. Holder, O. S. Jones, D. H. Kalantar, O. L. Landen, A. B. Langdon, S. Langer, B. J. MacGowan, A. J. Mackinnon, N. Meezan, E. I. Moses, C. Niemann, C. H. Still, L. J. Suter, R. J. Wallace, E. A. Williams and B. K. F. Young, Nature Physics **3**, 716 (2007).
- [40] S. H. Glenzer, L. J. Suter, R. E. Turner, B. J. MacGowan, K. G. Estabrook, M. A. Blain, S. N. Dixit, B. A. Hammel, R. L. Kauffman, R. K. Kirkwood, O. L. Landen, M.-C. Monteil, J. D. Moody, T. J. Orzechowski, D. M. Pennington, G. F. Stone, and T. L. Weiland, Phys. Rev.

- Lett. **80**, 2845 (1998).
- [41] S. H. Glenzer, L. M. Divol, R. L. Berger, C. Geddes, R. K. Kirkwood, J. D. Moody, E. A. Williams, and P. E. Young, Phys. Rev. Lett. **86**, 2565 (2001).
- [42] D. H. Froula, L. Divol, R. L. Berger, R. A. London, N. B. Meezan, D. J. Strozzi, P. Neumayer, J. S. Ross, S. Stagnitto, L. J. Suter, and S. H. Glenzer, Phys. Rev. Lett. **101**, 115002 (2008).
- [43] D. H. Froula, L. Divol, R. A. London, R. L. Berger, T. Döppner, N. B. Meezan, J. S. Ross, L. J. Suter, C. Sorce, and S. H. Glenzer, Phys. Rev. Lett. **103**, 045006 (2009).
- [44] E. Lefebvre, R. L. Berger, A. B. Langdon, B. J. MacGowan, J. E. Rothenberg, and E. A. Williams, Phys. Plasmas **5**, 2701 (1998).
- [45] J. D. Moody, B. J. MacGowan, J. E. Rothenberg, R. L. Berger, L. Divol, S. H. Glenzer, R. K. Kirkwood, E. A. Williams, and P. E. Young, Phys. Rev. Lett. **86**, 2810 (2001).
- [46] Y. Kato, K. Mima, N. Miyanaga, S. Arinaga, Y. Kitagawa, M. Nakatsuka, and C. Yamanaka, Phys. Rev. Lett. **53**, 1057 (1984).
- [47] R. L. Berger, C. H. Still, E. A. Williams, and A. B. Langdon, Phys. Plasmas **5**, 4337 (1998).
- [48] A. A. Offenberger, R. Fedosejevs, W. Tighe, and W. Rozmus, Phys. Rev. Lett. **49**, 371 (1982).
- [49] R. P. Paul, R. E. Turner, B. F. Lasinski, K. G. Estabrook, E. M. Campbell, C. L. Wang, D. W. Phillion, E. A. Williams, and W. L. Kruer, Phys. Rev. Lett. **53**, 1739 (1984).
- [50] J. D. Moody, P. Datte, K. Krauter, E. Bond, P. A. Michel, S. H. Glenzer, L. Divol, C. Niemann, L. Suter, N. Meezan, B. J. MacGowan, R. Hibbard, R. A. London, J. Kilkenny, R. Wallace, J. L. Kline, K. Knittel, G. Frieders, B. Golick, G. Ross, K. Widmann, J. Jackson, S. Vernon, T. Clancy, Rev. Sci. Instrum. **81**, 10D921 (2010).
- [51] S. H. Glenzer, F. B. Rosmej, R. W. Lee, C. A. Back, K. G. Estabrook, B. J. MacGowan, T. D. Shepard, and R. E. Turner, Phys. Rev. Lett. **81**, 365 (1998).
- [52] S. P. Regan, N. B. Meezan, L. J. Suter, D. J. Strozzi, W. L. Kruer, D. Meeker, S. H. Glenzer, W. Seka, C. Stoeckl, V. Y. Glebov, V. Yu, T. C. Sangster, D. D. Meyerhofer, R. L. McCrory, E. A. Williams, O. S. Jones, D. A. Callahan, M. D. Rosen, O. L. Landen, C. Sorce, B. J. MacGowan, Phys. Plasmas **17**, 020703 (2010).
- [53] E. L. Dewald, K. M. Campbell, R. E. Turner, J. P. Holder, O. L. Landen, S. H. Glenzer, R. L. Kauffman, L. J. Suter, M. Landen, M. Rhodes, D. Lee, Rev. Sci. Instrum. **75**, 3759 (2004).
- [54] E. L. Dewald, S. H. Glenzer, O. L. Landen, L. J. Suter, O. S. Jones, J. Schein, D. Froula, L. Divol, K. Campbell, M. S. Schneider, J. Holder, J. W. McDonald, C. Niemann, A. J. Mackinnon, and B. A. Hammel Plasma Phys. Cont. Fusion **47**, 405 (2005).
- [55] M. B. Schneider, O. S. Jones, N. B. Meezan, J. L. Milovich, R. P. Town, S. S. Alvarez, R. G. Beeler, D. K. Bradley, J. R. Celeste, S. N. Dixit, M. J. Edwards, M. J. Haugh, D. H. Kalantar, J. L. Kline, G. A. Kyrala, O. L. Landen, B. J. MacGowan, P. Michel, J. D. Moody, S. K. Oberhelman, K. W. Piston, M. J. Pivovaroff, L. J. Suter, A. T. Teruya, C. A. Thomas, S. P. Vernon, A. L. Warrick, K. Widmann, R. D. Wood, B. K. Young, Rev. Sci. Instrum. **81**, 10E538 (2010).
- [56] N. B. Meezan, Inertial Fusion Science Application Conference (2011), Bordeaux, France.
- [57] E. Dattolo, L. Suter, M-C. Monteil, J-P. Jadaud, N. Dague, S. Glenzer and R. Turner, D. Juraszek, B. Lasinski, C. Decker, O. Landen, and B. MacGowan, Phys. Plasmas **8**, 260 (2001).
- [58] E. L. Dewald, M. Rosen, S. H. Glenzer, L. J. Suter, F. Girard, J. P. Jadaud, J. Schein, C. Constantin, F. Wagon, G. Huser, P. Neumayer, and O. L. Landen, Phys. Plasmas **15**, 072706 (2008).
- [59] R. E. Marshak, Phys. Fluids **1**, 24 (1958).
- [60] R. L. Kauffman, L. J. Suter, C. B. Darrow, J. D. Kilkenny, H. N. Kornblum, D. S. Montgomery, D. W. Phillion, M. D. Rosen, A. R. Thiessen, R. J. Wallace, and F. Ze, Phys. Rev. Lett. **73**, 2328 (1994).
- [61] R. Sigel, G. D. Tsakiris, F. Lavarenne, J. Massen, R. Fedosejevs, J. Meyer ter Vehn, M. Murakami, K. Eidmann, S. Witkowski, H. Nishimura, Y. Kato, H. Takabe, T. Endo, K. Kondo, H. Shiraga, S. Sakabe, T. Jitsuno, M. Takagi, C. Yamanaka, S. Nakai, Phys. Rev. Lett. **65**, 587 (1990).
- [62] P. Michel, L. Divol, R. P. J. Town, M. D. Rosen, D. A. Callahan, N. B. Meezan, M. B. Schneider, G. A. Kyrala, J. D. Moody, E. L. Dewald, K. Widmann, E. Bond, J. L. Kline, C. A. Thomas, S. Dixit, E. A. Williams, D. E. Hinkel, R. L. Berger, O. L. Landen, M. J. Edwards, B. J. MacGowan, J. D. Lindl, C. Haynam, L. J. Suter, S. H. Glenzer, and E. Moses, Phys. Rev. E **83**, 046409 (2011).
- [63] J. D. Moody, P. Michel, L. Divol, R. L. Berger, E. Bond, D. K. Bradley, D. A. Callahan, E. L. Dewald, S. Dixit, S. Glenn, M. J. Edwards, C. Haynam, N. Izumi, O. Jones, R. K. Kirkwood, W. L. Kruer, J. L. Kline, G. A. Kyrala, O. L. Landen, S. LePape, J. D. Lindl, B. J. MacGowan, N. B. Meezan, M. D. Rosen, M. B. Schneider, L. J. Suter, C. A. Thomas, R. P. J. Town, K. Widmann, E. A. Williams, L. J. Atherton, S. H. Glenzer, E. I. Moses, Nature Physics , (2012) *in print*.
- [64] P. M. Celliers, D. K. Bradley, G. W. Collins, D. G. Hicks, T. R. Boehly, W. J. Armstrong, Rev Sci. Instrum., **75**, 4916 (2004).
- [65] T. R. Boehly, V. N. Goncharov, W. Seka, S. X. Hu, J. A. Marozas, D. D. Meyerhofer, P. M. Celliers, D. G. Hicks, M. A. Barrios, D. Fratanduono, and G. W. Collins, Phys. Plasmas **18**, 092706 (2011).
- [66] J. D. Kilkenny, M. D. Cable, C. A. Clower, B. A. Hammel, V. P. Karpenko, R. L. Kauffman, H. N. Kornblum, B. J. MacGowan, W. Olson, T. J. Orzechowski, D. W. Phillion, G. L. Tietbohl, J. E. Trebes, B. Chrien, B. Failor, A. Hauer, R. Hockaday, J. Oertel, R. Watt, C. Ruiz, G. Cooper, D. Hebron, R. Leeper, J. Porter, J. Knauer, Rev. Sci. Instrum. **66**, 288 (1995).
- [67] A. A. Hauer, L. Suter, N. Delamater, D. Reiss, L. Powers, G. Magelssen, D. Harris, O. Landen, E. Lindemann, W. Hsing, D. Wilson, P. Amendt, R. Thiessen, R. Kopp, D. Phillion, B. Hammel, D. Baker, J. Wallace, R. Turner, M. Cray, R. Watt, J. Kilkenny, J. Mack, Phys. Plasmas **2**, 2488 (1995).
- [68] O. L. Landen, P. A. Amendt, L. J. Suter, R. E. Turner, S. G. Glendinning, S. W. Haan, S. M. Pollaine, B. A. Hammel, M. Tabak, M. D. Rosen, J. D. Lindl, Phys. Plasmas **6**, 2488 (1999).
- [69] R. E. Turner, P. Amendt, O. L. Landen, S. G. Glendinning, P. Bell, C. Decker, B. A. Hammel, D. Kalantar, D. Lee, R. Wallace, D. Bradley, M. Cable, R. S. Craxton, R. Kremens, W. Seka, J. Schnittman, K. Thorp, T.

- J. Murphy, N. Delamater, C. W. Barnes, A. Hauer, G. Magelssen, J. Wallace, Phys. Plasmas **7**, 333 (2000).
- [70] H. W. Herrmann, N. Hoffman, D. C. Wilson, W. Stoeffl, L. Dauffy, Y. H. Kim, A. McEvoy, C. S. Young, J. M. Mack, C. J. Horsfield, M. Rubery, E. K. Miller, Z. A. Ali, Rev. Sci. Instrum. **81**, 10D333 (2010).
- [71] A. L. Kritcher, T. Döppner, C. Fortmann, T. Ma, O. L. Landen, R. Wallace, and S. H. Glenzer, Phys. Rev. Letters **107** 015002 (2011).
- [72] Sangster, V. N. Goncharov, P. B. Radha, V. A. Smalyuk, R. Betti, R. S. Craxton, J. A. Delettrez, D. H. Edgell, V. Yu. Glebov, D. R. Harding, D. Jacobs-Perkins, J. P. Knauer, F. J. Marshall, R. L. McCrory, P. W. McKenty, D. D. Meyerhofer, S. P. Regan, W. Seka, R. W. Short, S. Skupsky, J. M. Soures, C. Stoeckl, B. Yaakobi, D. Shvarts, J. A. Frenje, C. K. Li, R. D. Petrasso, and F. H. Séguin Phys. Rev. Lett. **100**, 185006 (2008).
- [73] V. N. Goncharov, T. C. Sangster, T. R. Boehly, S. X. Hu, I. V. Igumenshchev, F. J. Marshall, R. L. McCrory, D. D. Meyerhofer, P. B. Radha, W. Seka, S. Skupsky, C. Stoeckl, D. T. Casey, J. A. Frenje, R. D. Petrasso, Phys. Rev. Lett. **104**, 165001 (2010).
- [74] J. A. Frenje, D. T. Casey, C. K. Li, F. H. Séguin, R. D. Petrasso, V. Yu. Glebov, P. B. Radha, T. C. Sangster, D. D. Meyerhofer, S. P. Hatchett, S. W. Haan, C. J. Cerjan, O. L. Landen, K. A. Fletcher, and R. J. Leeper, Phys. Plasmas **17**, 056311 (2010).
- [75] H. Brysk, Plasma Physics **15**, 611 (1973).
- [76] V. Y. Glebov et al., Rev. Sci. Instrum. 81, 10D325 (2010); V. Y. Glebov et al., Rev. Sci. Instrum. **77**, 10E715 (2006).
- [77] M. M. Marinak, G. D. Kerbel, N. A. Gentile, O. Jones, D. Munro, S. Pollaine, T. R. Dittrich, S. W. Haan, Phys. of Plasmas **8**, 2275 (2001).
- [78] P. T. Springer, C. Cerjan, R. Betti, J. A. Caggiano, M.J. Edwards, J.A. Frenje, V.Yu. Glebov, S. M. Glenn, N. Izumi, O. Jones, G. Kyrala, T. Ma, J. McNaney, M. Moran, D. H. Munro, S. Regan, T.C. Sangster, S. Sepke, H. Scott, R. P. J. Town, S. V. Weber, B. Wilson, J. Physics (2012) submitted.
- [79] L. J. Suter, S. Glenzer, S. Haan, B. Hammel, K. Manes, N. Meezan, J. Moody, M. Spaeth, and L. Divol, K. Oades and M. Stevenson, Phys. Plasmas **11**, 2738 (2004).
- [80] C. Niemann, R. L. Berger, L. Divol, D. H. Froula, O. Jones, R. K. Kirkwood, N. Meezan, J. D. Moody, J. Ross, C. Sorce, L. J. Suter, and S. H. Glenzer, Phys. Rev. Lett. **100**, 045002 (2008).
- [81] M. Keilhacker and the JET Team, Plasma Phys. Control. Fusion **41** B1B23 (1999).
- [82] M. Keilhacker, A. Gibson, C. Gormezano, P.J. Lomas, P.R. Thomas, M.L. Watkins, P. Andrew, B. Balet, D. Borba, C.D. Challis, I. Coey, G.A. Cottrell, H.P.L. De Esch, N. Deliyanakis, A. Fasoli, C.W. Gowers, H.Y. Guo, G.T.A. Huysmans, T.T.C. Jones, W. Kerner, R.W.T. Konig, M.J. Loughlin, A. Maas, F.B. Marcus, M.F.F. Nave, F.G. Rimini, G.J. Sadler, S.E. Sharapov, G. Sips, P. Smeulders, F.X. Soldner, A. Taroni, B.J.D. Tubbing, M.G. von Hellermann, D.J. Ward, JET Team, Nuclear Fusion **39**, 209 (1999).
- [83] E. A. Lazarus, G. A. Navratil, C. M. Greenfield, E. J. Strait, M. E. Austin, K. H. Burrell, T. A. Casper, D. R. Baker, J. C. DeBoo, E. J. Doyle, R. Durst, J. R. Ferron, C. B. Forest, P. Gohil, R. J. Groebner, W. W. Heidbrink, R.-M. Hong, W. A. Houlberg, A. W. Howald, C.-L. Hsieh, A. W. Hyatt, G. L. Jackson, J. Kim, L. Lao, C. J. Lasnier, A. W. Leonard, J. Lohr, R. J. La Haye, R. Maingi, R. L. Miller, M. Murakami, T. H. Osborne, L. J. Perkins, C. C. Petty, C. L. Rettig, T. L. Rhodes, B. W. Rice, S. A. Sabbagh, D. P. Schissel, J. T. Scoville, R. T. Snider, G. M. Staebler, B. W. Stallard, R. D. Stambaugh, H. E. St. John, R. E. Stockdale, P. L. Taylor, D. M. Thomas, A. D. Turnbull, M. R. Wade, R. Wood, and D. Whyte, Phys. Rev. Lett. **77**, 2714 (1996).
- [84] E. A. Lazarus, G. A. Navratil, C. M. Greenfield, E. J. Strait, M. E. Austin, K. H. Burrell, T. A. Casper, D. R. Baker, J. C. DeBoo, E. J. Doyle, R. D. Durst, J. R. Ferron, C. B. Forest, P. Gohil, A. W. Hyatt, G. L. Jackson, J. Kim, L.L. Lao, C. J. Lasnier, A. W. Leonard, J. M. Lohr, R. J. La Haye, R. Maingi, R. L. Miller, M. Murakamp, T. H. Osborne, L. J. Perkins, C. C. Petty, C. L. Rettig, T. L. Rhodes, B. W. Rice, S. A. Sabbagh, D. P. Schissel, J. T. Scoville, R. T. Snider, B. W. Stallard, R. D. Stambaugh, H. E. St. John, R. E. Stockdale, P. L. Taylor, T. S. Taylor, D. M. Thomas, A. D. Turnbull, M. R. Wade, R. D. Wood, and D. G. Whyte, Nuclear Fusion **37**, 7 (1997).

TABLE I: Experiments on the National Ignition Facility with layered thermonuclear fuel. Error bars are discussed in the text. Fast rise pulse shapes are indicated with *.

Campaign	Shot Number	Laser Energy (MJ)	Peak Power (TW)	Hohl. scale	LEH dia. (mm)	Capsule dopant (% D)	Fuel	Y_F	T_i	ρR (g cm $^{-2}$)	DT	T_i	ρR	Yield
												Exp/ Sim	Exp/ Sim	Exp/ Sim
Commissioning	N100929	1.05	297	544	3.1	Ge	6	1.07	1.98	0.56	7.6×10^{12}			
Commissioning	N110121	1.05	302	544	3.1	Ge	6	0.74	2.48	0.56	2.1×10^{13}			
Commissioning	N110201*	1.24	383	544	3.1	Ge	6	0.8	3.70	0.54	1.1×10^{14}			
Commissioning	N110212*	1.30	397	544	3.1	Ge	6	0.66	3.61	0.57	1.3×10^{14}			
Shock timing	N110603	1.32	419	544	3.1	Ge	20	0.81	2.64	0.91	6.5×10^{13}	0.95	1.06	0.32
Shock timing	N110608	1.33	428	544	3.1	Ge	50	0.89	3.11	0.91	1.9×10^{14}	1.03	0.85	0.19
Shock timing	N110615*	1.33	431	544	3.1	Ge	50	0.96	3.32	0.74	4.3×10^{14}	1.09	0.91	0.49
Shock timing	N110620	1.42	434	544	3.1	Ge	50	1.18	4.27	0.89	4.2×10^{14}	1.4	0.77	0.30
Velocity	N110804	1.30	419	575	3.1	Si	2	0.92	2.73	0.69	4.8×10^{12}			
Velocity	N110826	1.41	425	575	3.1	Si	50	0.79	2.97	0.81	1.7×10^{14}	0.87	0.99	0.12
Velocity	N110904	1.44	426	575	3.1	Si	50	1.1	3.52	0.98	4.6×10^{14}	0.98	0.83	0.11
Velocity	N110908	1.43	423	575	3.1	Si	50	0.89	3.55	0.94	5.9×10^{14}	0.99	0.75	0.13
Velocity	N110914	1.62	432	575	3.1	Si	50	1.15	3.59	1.03	5.7×10^{14}	0.90	0.85	0.08
Shape	N111029	1.20	424	575	3.375	Si	2	0.91	2.84	0.82	9×10^{12}			
Shape	N111103	1.21	422	575	3.375	Si	50	0.97	3.28	0.95	2.3×10^{14}			
Shape	N111112	1.45	428	575	3.375	Si	50	0.98	3.90	0.93	6.0×10^{14}			
Shape	N111215	1.40	416	575	3.375	Si	50	0.89	3.53	0.94	7.5×10^{14}			